Appendix C—Deformation Models for UCERF3

By Tom Parsons,[1] Kaj M. Johnson,[2] Peter Bird,[3] Jayne Bormann,[4] Timothy E. Dawson,[5] Edward H. Field,[1] William C. Hammond,[4] Thomas A. Herring,[6] Rob McCaffrey,[7] Zhen-Kang Shen,[3] Wayne R. Thatcher,[1] Ray J. Weldon, II,[8] and Yuehua Zeng[1]

Summary

This document describes efforts to best characterize seismogenic deformation in and near California. The rate of hazardous earthquakes in California is expected to be proportional to deformation rates; in particular, the rates at which faults slip. Fault slip rates are determined from offsets of geologic and geomorphic features of measured age and by modeling geodetically determined surface displacement rates. Extensive use of geodesy in the form of Global Positioning System (GPS) observations is a new feature brought into the Working Group on California Earthquake Probabilities (WGCEP) forecasts for the Uniform California Earthquake Rupture Forecast, version 3 (UCERF3) model. Geodetic measurements are potentially more spatially comprehensive than geologic offset observations, which can be clustered. Applying either type of data is subject to considerable uncertainty. Geologic observations have dating and other measurement errors, and they often must be extrapolated long distances on fault sections. However, geodetic observations require a modeling step to translate them into estimates of fault slip rate, and they have poor resolution on closely spaced, locked faults. Details about fault slip rates from geologic offsets are presented in appendix B (this report). In this appendix we look at three deformation models that use geologic and geodetic constraints and compare/contrast them with the UCERF3 geological model and the UCERF2 deformation model. We present models, results, and evaluation for their use in the UCERF3 forecast.

We identify here two classes of geodetic models for fault slip rate and residual "off-fault" seismogenic deformation: (1) elastic block models and (2) what we call faulted continuum models. Both fit the observed data reasonably well, and are viable representations of California deformation. Generally, the geodetic models give high weight to geologic information and change it only enough to also fit GPS and stress-direction observations. In so doing, they modify the geologic model to be more consistent with the overall relative plate-motion vectors across the Pacific-North American Plate boundary region in California. The faulted continuum models tend, like the geologic model, to have uniform slip along strike for most faults. One block model,

[1] U.S. Geological Survey.
[2] University of Indiana.
[3] University of California, Los Angeles.
[4] University of Nevada, Reno.
[5] California Geological Survey.
[6] Massachusetts Institute of Technology.
[7] Portland State University.
[8] University of Oregon.

called here the average block model because it has resulted from a separate inversion of results from five different techniques, is the model that shows more slip-rate gradients on major faults relative to the other models. We examine the proposed UCERF3 deformation models in the contexts of (1) overall moment rate, (2) fit to GPS observations, (3) fit to geological constraints, (4) fit to relative plate-motion rates and directions, and (5) magnitudes of residual moment rate not on defined faults.

We developed weighting schemes based on the ranking presented in the summary table (table C1) and from expert opinion developed through the UCERF3 Deformation Model Evaluation Committee. There are data-driven differences for slip-rate estimates on important faults like the southern San Andreas such that a range of models based on the geologic and geodetic data can define the deformation rates for use in earthquake rate estimates.

Table C1. Overview of model performance ranking against a variety of tests and measures as described in sections on deformation model results and model weighting of this appendix.

[ABM, averaged block model; NeoKinema, a finite-element model by Bird and Liu (2007); Zeng-Shen is a buried dislocation model by Yuehua Zeng and Zhen-Kang Shen; Geological, the UCERF3 geological deformation model (appendix B, this report)]

	ABM	NeoKinema	Zeng-Shen	Geological
			Rank	
1. Total Moment Rate				
(a) Moment rate on faults	2	1	1	2
(a) Total moment rate	3	2	1	3
Averaged rank	3	2	1	3
2. GPS Fit				
(a) Normalized χ^2	3	1	2	4
(b) Residuals - Urban regions	2	1	3	N/A
Averaged rank	2	1	2	3
3. Slip on faults w.r.t. geology				
(a) Rake reversals	3	2	1	1
(b) Overall fit to geo rates	3	4	2	1
(c1) Slip rate continuity	4	2	3	1
(d) Subsections out of geo bounds	3	4	2	1
(e) Subsections out of geo bounds with best constraints	4	3	2	1
(f) Subsections out of geo bounds high slip rates	3	2	4	1
Averaged rank	3	3	2	1
4. Line integral paths	1	1	2	3
5. Background, residual deformation	3	1	2	4
Sum of ranks (lower is better)	12	8	9	14

Contents

Introduction

Forecasting earthquakes in California depends on measurements, estimates, and models of fault slip rates. The rate at which faults slip, when combined with magnitude-area relationships and magnitude frequency distributions, controls the majority of calculated earthquake rates in the Uniform California Earthquake Rupture Forecast (UCERF). In addition to fault slip rates, identified crustal deformation not associated with known faults (termed "off-fault deformation" in the UCERF parlance) contributes to the earthquake hazard. Fault slip rates and off-fault deformation are assembled from geologic information, such as datable offset markers that can be tied across a fault, and from modeling-space geodetic measurements like Global Positioning System (GPS) observations. GPS can also be used to identify off-fault deformation, as can historical and current seismicity.

The purpose of this appendix is to provide details about (1) the methods the UCERF3 forecast has developed to estimate seismogenic deformation, (2) why these methods have been used, (3) results from and some implications of the different deformation models, and (4) factors and criteria applied in weighting deformation models. All input data applied for deformation modeling/estimates can be found at *http://wgcep.org/data*.

Four quasi-independent approaches to estimating California seismogenic deformation are intended for use in UCERF3: all are weighted here and three are presented in detail: (1) a finite element method (NeoKinema), (2) an average of five elastic block modeling methods (ABM), and (3) a buried dislocation approach that has been used by the National Sesimic Hazard Map Program (NSHMP). A fourth model is called the geologic model, which has no geodetic constraints and is described in appendix B (this report).

This appendix is organized into an initial discussion of the available data and justification of the rationale behind the UCERF3 deformation approach, followed by detailed descriptions of new methods that have not been previously used by the Working Group on California Earthquake Probabilities (WGCEP) or in past UCERF efforts. Finally, a general discussion of results is presented (complete results are appended in tabular form), and a model weighting strategy is presented.

Data: Why Geologic and Geodetic Models?

Earthquake forecasts are necessarily an underinformed process. We have not witnessed enough earthquakes anywhere in the world to make accurate forecasts based solely on historical catalogs. Previous models by the WGCEP, National Seismic Hazard Map Program (NSHMP), and UCERF have thus been assembled from all possible data that can inform earthquake rate calculations. A major dataset, geodetic observations of earth surface velocity, has yet to be employed in a systematic way. Comparison between figure C1 (GPS data spatial distribution) and figures C2 and C3 (geologic sites for fault slip rates) shows how much more completely sampled the state of California is geodetically. Therefore, an opportunity presents itself to add

deformation observations where none existed previously. The challenge is to use the geodetic and geologic data in the best, most complementary way.

UCERF2 slip rates were assigned on the basis of an expert-opinion evaluation of available data (mostly geologic and geodetic), together with summations across various transects to make sure the total plate-tectonic rate was matched (Field and others, 2009). Figure C4 shows residual velocities between observed GPS velocities and predicted velocities based on the UCERF2 deformation model. Those residuals are quite large, particularly in the Transverse Ranges, Mojave, the east California shear zone, and near Parkfield and the San Francisco Bay area. The question is whether more quantitative models based on inversion of geodetic and geologic observation with the total plate-rate constraints could be used to improve upon the UCERF2 models.

In UCERF3, fault slip rates and off-fault strain rates estimated from inversions of GPS-derived velocities and geologic slip rates with kinematic models compete conceptually with expert-opinion rates. UCERF3 deformation models do not have type C zones (areas of diffuse deformation, of which 50 percent was presumed to be seismogenic in UCERF2), and all faults are assigned slip rates. Deformation models provide the strain rate tensor on a 0.1 degree by 0.1 degree grid covering all of California. This grid of strain rates account for all modeled deformation that is not accommodated on the faults.

GPS Velocity Field

All kinematic models were constrained by a UCERF3-consensus GPS velocity field constructed by Thomas Herring (T. Herring, written commun.,). This velocity field was generated by combining velocity fields submitted by 10 GPS analysis groups (see table C1). The Stable North America Reference Frame formed the basis for the combination. The methods and issues in the generation of the consensus field are associated with data quality, reconciliation of the error models used by different groups to generate the uncertainties of the velocity estimates, and the treatment of the nonsecular motions. The combination aligns each solution to a common reference frame, removing velocity estimates that are inconsistent with other solutions. Overall, 276 velocity estimates were removed in the current analysis. Inconsistent sites mainly arise in areas of postseismic deformation and at sites that have substantial nonsecular motion components, due often to ground water and sometimes to antenna failures. Relative uncertainties in the solutions are approximately correct in most cases. Current improvement is to compare each solution to a combination of the other solutions (with discordant sites removed) and to fit a noise model of the form:

$$s^2 = s^2_{min} + k s^2_{rep}$$

where s^2_{min} and k are constants to be estimated and s^2_{rep} is the reported velocity variance. The constants are determined from the c2 distribution of the residuals. Results from the combination show $s_{min} \sim 0.3$ mm/yr, with variance scale factor, k, between 1 and 4, depending on analysis group. The latest velocity field sent to the UCERF3 working group is designated with time tag of GPS week 1638, June 2011.

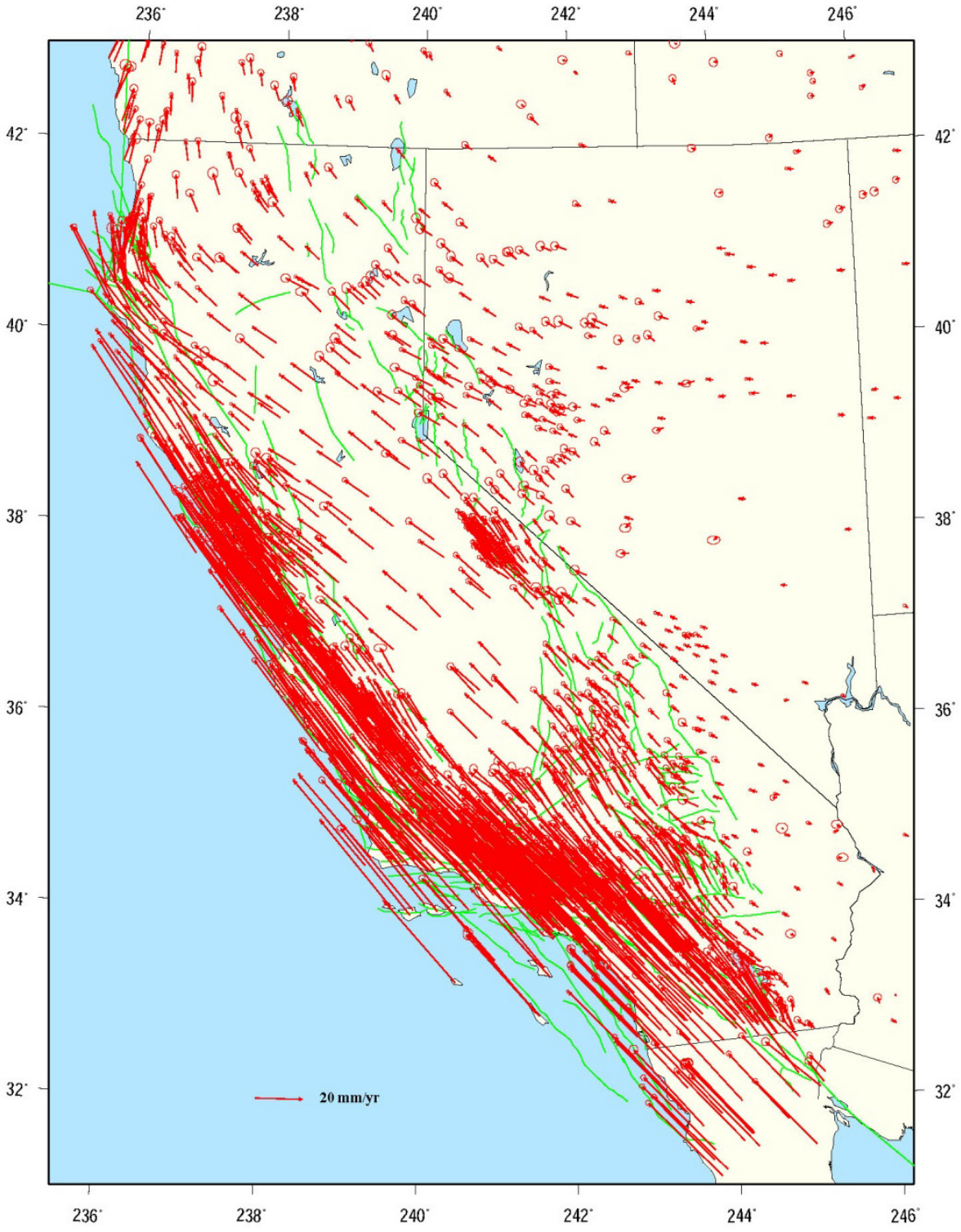

Figure C1. Map showing distribution of UCERF3 GPS velocity vectors for California and its neighbors, referenced to the North American Plate. Error ellipses represent 50-percent confidence.

Table C2. Fit of individual contributions (sources) to the combination of all other contributions to the UCERF3 consensus velocity model. For each contribution, the table gives the number of stations common to the other contributions, the Weighted Root-Mean-Square (WRMS) difference between the velocity estimates, and the $\sqrt{\chi^2 / f}$ of the differences. Further iterations of the solution reweighting should bring the $\sqrt{\chi^2 / f}$ values to unity.

Source	Common sites	WRMS (mm/yr)	$\sqrt{\chi^2 / f}$
NASA MEASURES	1,093	0.58	0.81
NGS CORS	598	0.74	0.89
PBO to June 2011	1,392	0.61	1.26
McCaffrey PNW	301	0.76	0.95
SCEC CMM4	583	0.8	1.08
Canadian Base Network	43	0.46	0.97
NA Reference Frame	341	0.58	1.1
UCLA Western US	1,447	0.51	0.93
U. Nevada Western US	1,096	0.43	1.02
USGS Western US	1,275	0.97	1.21

Geologic Slip Rates

Geologic slip rates at points shown in figure C2 were used as data to constrain all of the kinematic inversions and, consequently, the UCERF3 geologic model. There are two fault models (FM3.1 and FM3.2), and all solutions are computed twice. Depending on how many deformation model classes are used in UCERF3, there will be twice that number of deformation models as a result. The geologic slip rates are taken from the UCERF3 compilation (appendix B, this report). That is a compilation of slip rate estimates from the published literature along with an evaluation of the quality of the estimate, which varies substantially from one site to the next. The quantity of rates reported for each geologic site also varies. Some studies report upper and lower bounds on slip rates, other studies provide only a minimum or maximum, and some studies report a preferred rate. Figure C2 summarizes the geologic slip rate observation sites. These data are implemented as constraints differently in the various kinematic models. Some kinematic models use the reported uncertainties as standard deviations in a Gaussian distribution, while others treat these data as strict upper and (or) lower bounds.

In response to initial modeling efforts that used geologic slip rates as input constraints, a linear taper was applied to selected high-slip-rate faults where they overlap; this was done where significant departures from relative plate motions resulted, most notably on Salton Trough faults (Cerro Prieto, Imperial). In the following three sections, details about the methods used to model geodetic and geologic data are presented.

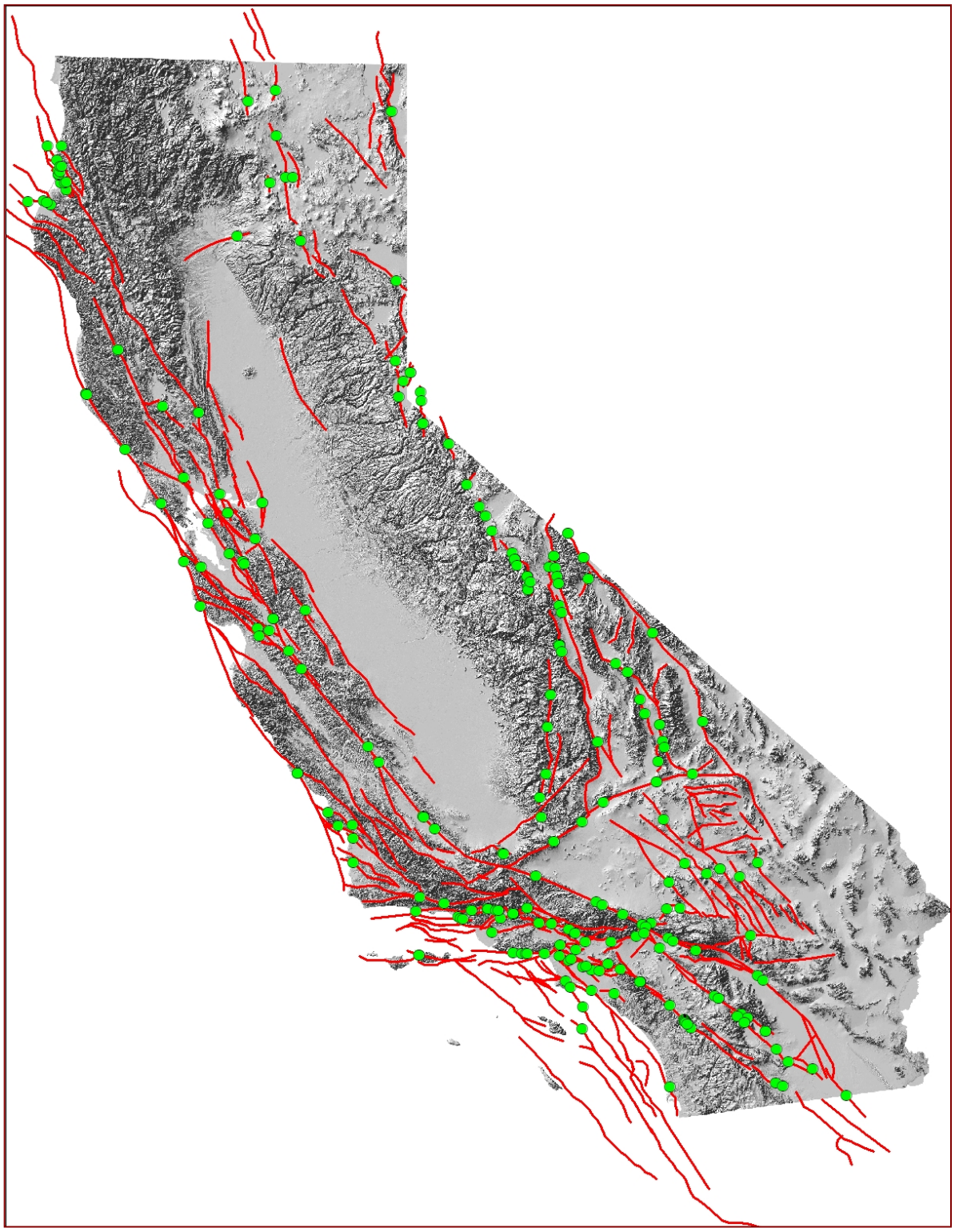

Figure C2. Geologic slip-rate data. Map view of the geologic sites (green dots) used for the block-like model. Red lines are UCERF3 fault traces.

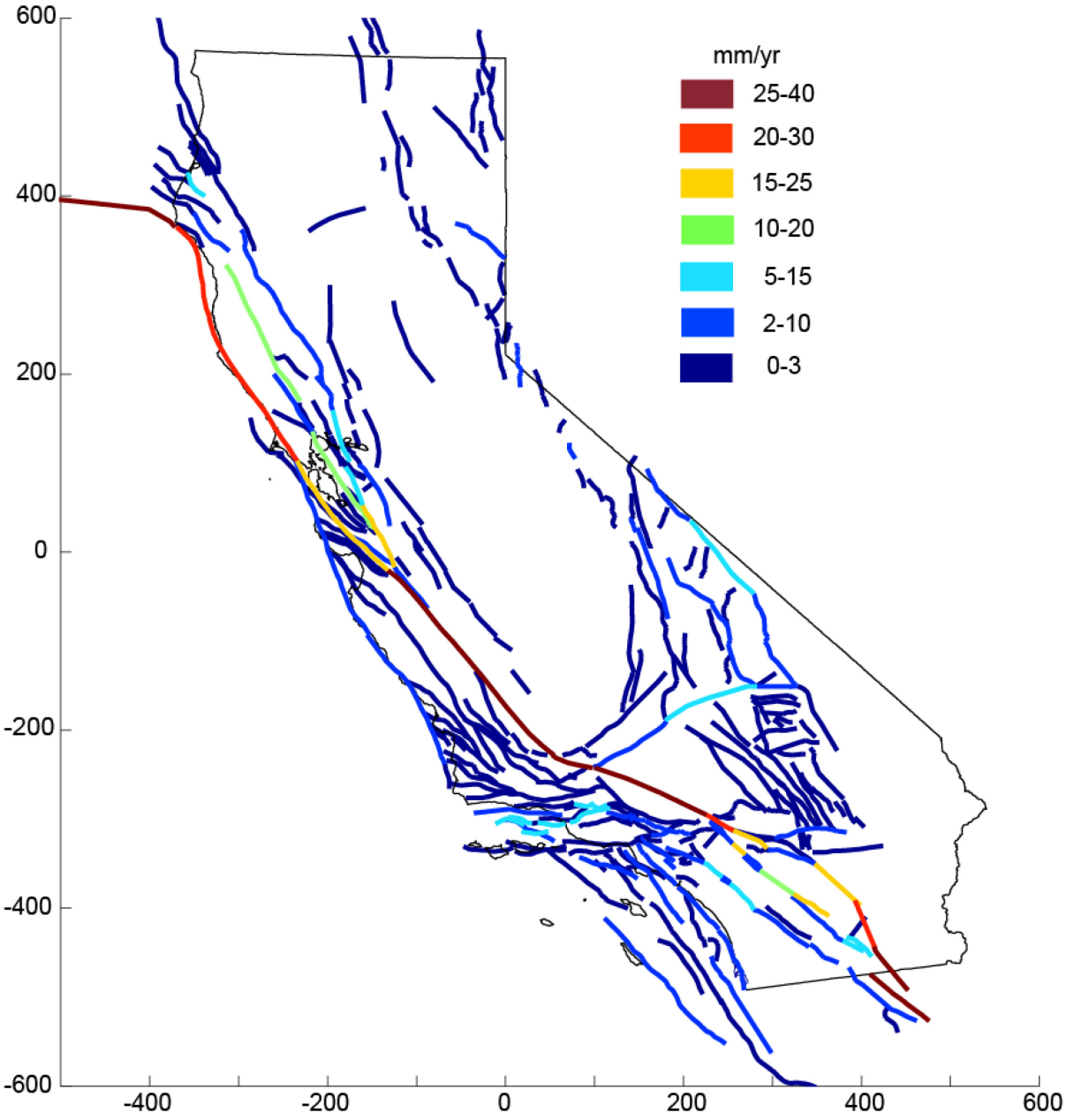

Figure C3. Map showing the geologic bounds (appendix B, this report) used to constrain the Geologic Block Model. Estimated slip-rates are shown on these bounding faults. Distances are given from 120˚W and 37˚N.

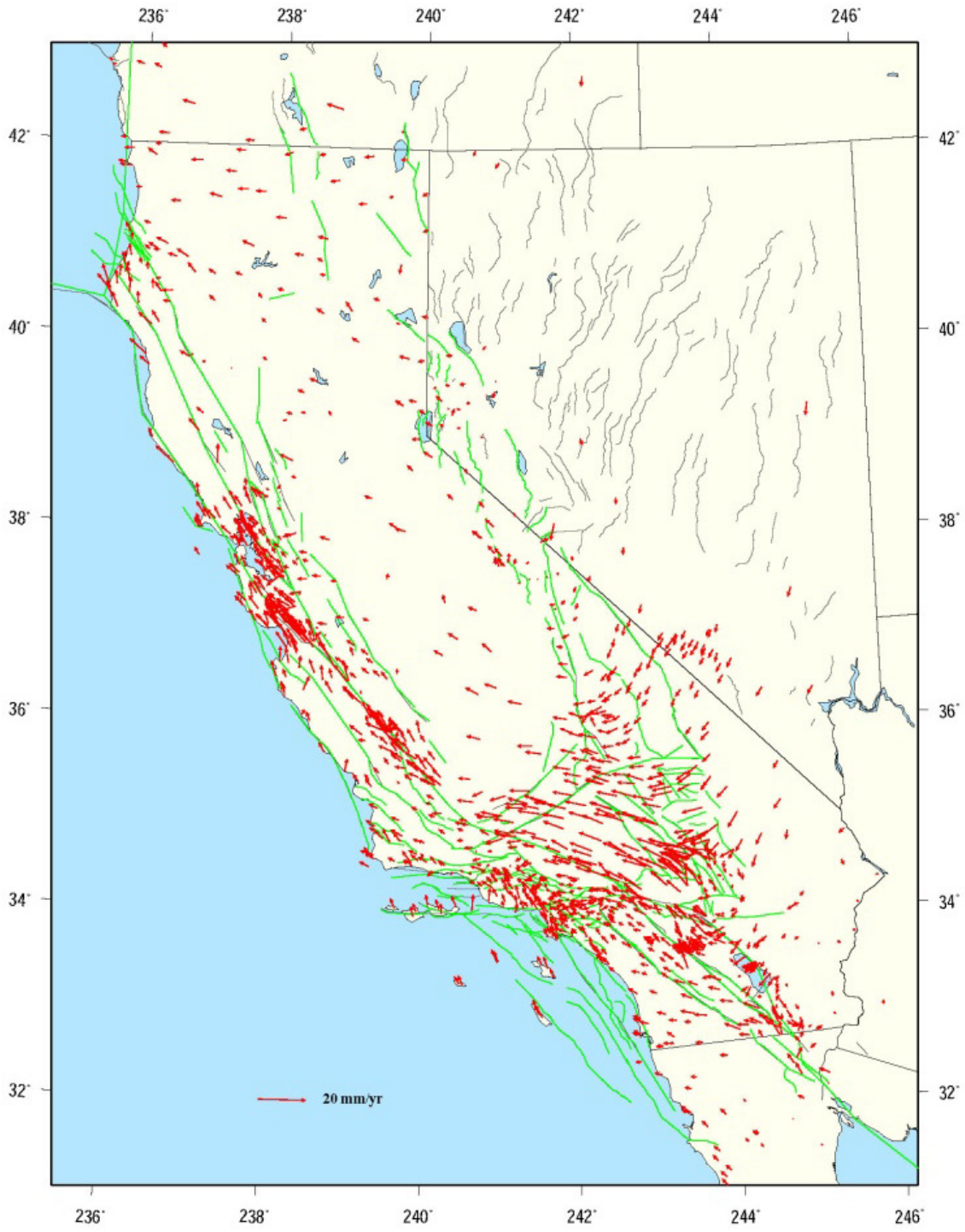

Figure C4. Map showing residual velocities between the observed Global Positioning System (GPS) velocities and model prediction from the UCERF2 deformation model. The residual vectors are plotted at the same scale as the observed GPS velocities in figure C1.

The NeoKinema Model

Overview

Geodetic studies over the past century have shown that velocities of benchmarks near the most active faults are not steady because of cycles of elastic strain accumulation and release in earthquakes and (or) creep events. Extrapolating this result to faults with mean slip rates of 1 mm/yr or less, we expect that velocities adjacent to such faults might vary significantly if averaged over less than 10^4 years. At longer time scales, plate tectonic models based on marine magnetic anomalies show that large plates change their velocities on a scale of 10^7 years because of the birth and death of spreading ridges, subducting slabs, and other plate-boundary features. The smaller plates within complex orogens (Bird, 2003) might be expected to show important velocity variations on a scale of 10^6 years because less relative deformation of faults is needed to significantly change the shape of a small plate. However, it is reasonable to expect that, if surface velocities could be measured over scales of 10^4 to 10^6 years, they would be stable in most regions. This is the long-term average velocity field that we seek to estimate with program NeoKinema.

NeoKinema applies geologic constraints at the points where they are measured, and attempts to maintain constant slip on faults as they cross model elements. However, it will adjust slip rates along strike if necessary to achieve better fit to other data constraints.

The kinematic finite-element code NeoKinema.f90 has been tested in a number of previous modeling studies, including Bird and Liu (2007), Liu and Bird (2008), Bird (2009), and Howe and Bird (2010). The equations underlying the program were presented in Supplemental Material S1 (sm001.pdf) of Liu & Bird (2008). This algorithm merges geologic offset rates, geodetic velocities, and principal stress directions to estimate the long-term velocity field at the top of the crust. The model domain is the area within a closed curve on the Earth's spherical surface. The degrees of freedom at each node of the finite-element mesh of triangles are the southward and eastward components of long-term-average velocity. Differentiation of velocity within each triangle yields the long-term-average 2-D (horizontal plane) strain-rate tensor, which is permanent (not elastic) by definition. The remaining components of the 3-D permanent strain-rate tensor are derived from conservation of volume and verticality of one principal axis.

The method of solving for nodal horizontal velocity components is to optimize a weighted-least-squares objective function by finding its stationary point in multidimensional velocity-component space with a system of linear equations. Nonlinearities are handled by iterating the solution 20 times in each run.

Geodetic benchmarks are treated as internal point constraints (with uncertainties) on the velocity field. However, geodetic velocities are first corrected to remove temporary velocity anomalies due to local elastic bending around temporarily locked seismogenic portions of (most) faults, using the current model estimates of the fault slip rates, locking depths assigned a priori, and analytic solutions for rectangular dislocations in a uniform elastic half-space. This requires iteration.

To first order, the strain rates and fault slip rates obtained from derivatives of the long-term average velocity field should be free of elastic strain contributions and result instead from permanent strain mechanisms, such as frictional sliding in the upper crust and dislocation creep in the lower crust. Therefore, it is also reasonable to expect that long-term average strain rates in the upper lithosphere should be proportional to long-term average seismic moment production. The necessary conversion factors are the elastic shear modulus (which is well known) and the

coupled lithosphere thickness contributing to seismicity, which has been estimated by Bird and Kagan (2004) based on 20th-century seismicity. Thus, results from NeoKinema lead directly to stationary models of long-term average seismicity and seismic hazard.

Objective Function

In many inverse problems the data are discrete, because they come from measurements at distinct points. Assume that all data that constrain velocity or strain rate at particular points have been transformed to scalar rate estimates r_k. (Subscript k = 1,..., K identifies the scalar datum, which is typically one horizontal component of long-term average velocity derived from a geodetic benchmark velocity.) Let the corresponding scalar rate predictions derived from the velocity field of the model be called p_k. Assume that each scalar rate r_k has an uncertainty that can be approximated by a Gaussian probability distribution with standard deviation σ_k, and assume temporarily that the errors in these rates are independent. Then the natural logarithm of the density of the joint probability that the model matches all the data is formed from the individual probability densities ϕ as:

$$S \equiv \ln\left\{\prod_{k=1}^{K}\Phi\left(p_k = r_k\right)\right\} = \sum_{k=1}^{K}\ln\left[\Phi\left(p_k = r_k\right)\right] = -\sum_{k=1}^{K}\left[\frac{\left(p_k - r_k\right)^2}{2\sigma_k^2} + \ln\left(\sigma_k\right) + \ln\sqrt{2\pi}\right] \quad (1)$$

and the part of this that is variable (with respect to changes in the model) is the familiar weighted-squares-of-prediction-errors criterion

$$S' \equiv -\sum_{k=1}^{K}\frac{\left(p_k - r_k\right)^2}{2\sigma_k^2} \quad (2)$$

which is to be maximized.

However, in the NeoKinema algorithm we also consider some constraints (geologic slip rates) to apply all along the trace of a fault and other constraints (minimization of strain rate, and isostropy) to apply all across the area of unfaulted continuum. There is no natural way of counting these constraints as discrete data (or pseudo-data), and no natural, correct weighting of these constraints against point data in the objective function. Instead, we leave this choice to the user of the program by introducing parameters called reference length L_0 and reference area A_0, which are used to maintain nondimensionality in a generalized objective function that includes both line and area integrals:

$$S'' \equiv -\sum_{k=1}^{K}\frac{\left(p_k - r_k\right)^2}{2\sigma_k^2} - \frac{1}{L_0}\sum_{m=1}^{M}\int_{length}\frac{\left(p_m - r_m\right)^3}{2\sigma_m^2}dl - \frac{1}{A_0}\sum_{n=1}^{3}\iint_{area}\frac{\left(p_m - r_m\right)^3}{2\sigma_m^2}da \quad (3)$$

where m = 1,..., M enumerates the target rates r associated with fault-slip degrees of freedom and n=1,2,3 enumerates the three target rates r_n associated with the three components of strain rates at each continuum point. The first term of this objective function includes the target velocities derived from geodetic benchmark-velocity data, the second term includes the targets derived from geologic slip-rate data, and the third term includes the targets derived from stress-direction data (and the stiff microplate assumption). Therefore, L_0 and A_0 can be considered as dimensional tuning parameters to be adjusted, by trial-and-error or systematic search, to equalize the fit of NeoKinema models to all three classes of data.

Finite Element Approximation

It is only necessary to estimate the horizontal components of the long-term average velocity, and it is only necessary to do this on the planet's surface. Therefore, we divide the area of the model into spherical-triangle finite elements (Kong and Bird, 1995) and solve for the horizontal components of velocity at each node. Long-term average velocities at other points are determined by interpolation, and long-term anelastic strain rates are determined by differentiation. (Where these elements are small, the surface of the sphere is locally almost flat, and the nodal functions of such elements are very close to those of plane-triangle constant- strain finite elements.)

Boundary Conditions

Only velocity boundary conditions are possible in NeoKinema. Stress is described only by orientation (but not magnitude) within the model domain, so stress (traction) boundary conditions are not available. However, if no velocity boundary condition is prescribed along a model edge, the effects will be similar to those of traction-free boundary conditions found in dynamic models. Such treatment would be appropriate if the model domain were limited to the overriding plate in a subduction zone for that part of the model boundary running along the trench.

Continuum Stiffness: the Microplate Constraint

An essential context for all the fault-related geologic data showing locally intense straining is that they should compete with an a priori assumption that in other places the strain-rate is close to zero. An appropriate formalism is to assign a zero target strain-rate, with a statistical uncertainty. A larger standard deviation could be attached to this null target rate in complex or poorly studied regions, where unknown faults might be buried and overlooked.

The particular scalar function of the strain-rate tensor that is used has the effect of causing unfaulted areas to behave as Newtonian viscous sheets of lithosphere in a state of plane stress. The NeoKinema algorithm will result in velocities that minimize the area integral of squared strain-rates for the unfaulted elements; this is exactly the result one would obtain by deriving a dynamic finite-element algorithm from the momentum equation (in the absence of horizontal boundary tractions or body forces), adopting a linear rheology, and solving for velocity with inhomogeneous boundary conditions.

Use of Stress Directions: the Isotropy Constraint

One principal stress direction must always be perpendicular to the free surface of a planet, or approximately vertical. Thus, the orientation of the stress tensor is well described by the azimuth of the most compressive horizontal principal stress. These directions are tabulated in data sets such as the World Stress Map.

Unfortunately, these data are very noisy. Variance in stress direction does not approach zero as pairs of data points are selected closer and closer together. Another problem is that the uncertainties assigned to individual directions are mostly generic estimates, not the result of repeated measurements at one point. A third problem is that there are spatial gaps in the datasets, such that many finite elements in a fine grid won't contain any data. To handle all these problems, we first interpolate observed stress directions to the center of each finite element, using an algorithm by Bird and Li (1996).

To use this information about stress in NeoKinema models, we approximate the lithosphere as horizontally isotropic, so that the principal directions of the strain-rate tensor in unfaulted continuum elements should be the same as the principal directions of stress. There may be an error of as much as 35° associated with this assumption if and where the lithosphere contains unrecognized weak faults. Even so, the solutions will be more accurate and reasonable than ones that ignore stress data and leave the orientations of continuum strain rates completely unconstrained. (Unconstrained models often show sinistral simple-shear straining adjacent to dextral strike-slip faults and extensional continuum straining adjacent to thrust faults. Such local reversals of stress are implausible and should be suppressed for a realistic simulation.)

Use of Fault Slip-Rate Data

NeoKinema solves for only the horizontal components of velocity at the surface, so a fault is treated as a surface discontinuity in horizontal velocity. The offset-rate parameter of greatest interest is the heave rate, which is the horizontal component of the slip rate. For convenience, and to reduce errors, specific fault types have been predefined, so that all fault-offset rates can be entered with positive numbers (and in conventional units of mm/yr). For the first four fault types, the heave rate is directly specified. Right-lateral and left-lateral faults have heave-rate vectors parallel to the fault trace. Divergent faults have heave rates at right angles to the trace, with an opening or spreading sense (examples include low-angle detachment faults, convex-upward rolling-hinge detachment faults, concave-upward listric normal faults, and rotating sets of planar bookshelf normal faults). For the two remaining fault types (planar thrusts and planar normal faults), the throw rate (vertical component of slip rate) is entered. For these last two types, a fault dip must be assumed so that NeoKinema can convert throw rates to heave rates.

Fault slip rate is, in general, a two-component vector. If both the dip-slip and the strike-slip components of the slip rate are known, NeoKinema treats these as two distinct scalar constraints along the same fault trace. When only the dip-slip rate is known, NeoKinema provides an option to permit limited strike slip in proportion to the amount of dip slip. (This is useful because otherwise a thrust fault with a complex trace could not slip without deforming its hanging wall and (or) footwall, and such deformation would be strongly resisted by the continuum stiffness constraint discussed above.) There is no corresponding provision for limited dip slip on known strike-slip faults, because strike-slip faults are modeled as vertically dipping, and thus any dip-slip component would not affect the horizontal velocity components estimated by NeoKinema.

When a fault is long enough to cross several finite elements, NeoKinema attempts to impose the same offset rate in all elements. In the case of rigid-microplate tectonics, where each fault connects to other faults at triple-junctions, this method is reasonably accurate. (The only difficulty occurs where there are rapid relative rotations of adjacent microplates, but this can be handled by segmenting the faults and varying the target rates along the strike of each fault.) The other end-member is the case where no faults connect, but all terminate within the domain. In that case, each fault might be expected (on the basis of crack theory for linear materials) to have an ellipsoidal profile of slip rate versus length. Such elliptical faults would have a mean offset rate that is only 79 percent ($\pi/4$) of their maximum offset rate. Thus, NeoKinema might overstate fault-related strain-rates by 27 percent in some cases where faults do not connect and where the geologic offset rates reported are all maxima along their respective traces. However, if

the geologic offset rates were determined at random points of convenience, then once again no systematic error is expected.

For each finite element containing one or more fault traces, there are four steps: (a) Form the target strain-rate tensor for that element as the sum of the strain-rate tensors implied by all the active fault segments cutting that element. (b) Form the matrix of covariances of the strain-rate components in that element as the sum of the covariances added by all the active fault segments, plus the small covariance of the strain-rate in the continuum around them. (c) Diagonalize the covariance matrix to find its three principal axes (in strain-rate space) along which the uncertainties are independent, and rotate the target strain-rates into this new coordinate system. (d) Add these three independent targets as scalar data with known uncertainties in the global system of equations.

Version 3 of NeoKinema (used in UCERF3.2 and later deformation models) includes a feature allowing for hard lower and upper limits on the offset rate of each modeled fault. This was used to set a lower limit of zero (or higher) for each offset component of each fault, so that none could slip with the wrong sense. (Correct senses were inferred from the generic rake angles specified in UCERF3 fault models FM3.1 and FM3.2.) In the cases of faults that have at least one dated offset feature, upper limits (and, usually, positive lower limits), an offset rate was also specified. These were based either on the limits given in the UCERF3 Geologic Model, or on the 95-percent confidence bounds computed by Bird (2007, tables 1 & 2) or Bird (2009, table 4). Preference was given to the bounds from the UCERF3 Geologic Model whenever these limits were similar to, or broader than, the published limits.

Use of Geodetic Data

Equations 1 through 3 already provide for the incorporation of geodetic velocity components at benchmarks, but only in certain ideal cases. Three practical difficulties often arise: (a) The two velocity components at one benchmark and (or) the velocities at different benchmarks have correlated uncertainties. (b) The relation between the velocity reference frame for the geodetic velocities and that of the velocity boundary conditions may be uncertain. (This occurs when all, or almost all, of the benchmarks used in the geodetic velocity solution are located within an orogen and few or none are outside the orogen on rigid plates.) (c) Geodetic velocities at benchmarks near active faults do not represent long-term average velocities because the faults remain locked, or else suddenly slip by large amounts, during the period of observation.

Correlated uncertainties in geodetic velocity components (problem a) violate the assumption of independence used to obtain the simple objective function in equation 2. Therefore, coordinates must be rotated to new variable space of the same dimensionality, in which the uncertainties are independent, and prediction errors should be evaluated in those new coordinates. It is well known that equation 2 should be replaced by:

$$S' \equiv \frac{1}{2}\sum_{j=1}^{K}\sum_{k=1}^{K}\left(p_k - r_k\right)N_{jk}\left(p_j - r_j\right) \tag{4}$$

where the normal matrix $\tilde{N}$ is the inverse of the covariance matrix $\tilde{C}$ of the observed velocity components $\vec{r}$.

If any fault is creeping steadily (such as the central segment of the San Andreas Fault in California), this fault is flagged with a logical switch on input, and corrections to geodetic

velocities at benchmarks will not include any coseismic contribution from that fault. We do not currently have any algorithm to handle intermediate cases of combined fault creep and coseismic offset on the same fault.

Iterative Improvement

At four points in the algorithm described above, we referred to the use of model estimates from a previous iteration to improve the solution. All of these iterations are combined and performed simultaneously, with forty-five iterations per run.

Manual Edits

NeoKinema (v. 3) models were computed in January 2013 at the University of California, Los Angeles (UCLA), for use as candidate deformation models in both UCERF3, and the 2014 release of the National Seismic Hazard Map by the U.S. Geological Survey (USGS) (NSHM2014). The predictions of these models concerning fault slip rates received a lot of scrutiny, both through individual efforts and through four days of "fault-by-fault" review meetings in January-February 2013 at Menlo Park and Pasadena, California.

In most cases where the geologic-model slip rates were based on dated offset features, the associated upper and lower limits on fault-offset rates were enforced in NeoKinema calculations. As a result, there were some differences in preferred value, but no glaring discrepancies. The biggest discrepancies in this group occurred where there was only a geologic constraint on the dip-slip component of faulting, and the geologic model made a simplifying assumption of zero strike-slip. Since NeoKinema does not share this assumption, it sometimes predicts a slip rate higher than the upper geologic bound, while honoring the actual geologic datum or data concerning rates of dip-slip.

However, a large fraction of the geologic slip rates (and slip rate bounds) were not based on any dated offset features (or did not appear to be based on dated offset features). These cases are more troublesome. In these cases, the geologic model typically assigns slip-rate bounds based on the date of the most recent ground-breaking rupture, expressed as a geologic epoch (for example, Holocene or Latest Pleistocene or Middle Quaternary), which itself is typically a subjective estimate based on scarp morphology, soil color, and other nonquantitative measures. If there is no evidence for Holocene surface ruptures, the geologic model typically assumes that there has been no surface rupture in the Holocene (which does not necessarily follow by strict logic) and therefore assigns a maximum slip rate of 0.2 mm/yr (for example, 2 m in 10,000 years). The preference is to leave these slip rates free to be assigned by the NeoKinema modeling process, based on GPS velocities, kinematic compatibility, and regional stress directions. This pair of contrasting strategies is potentially appropriate for representation in a logic-tree, with the NeoKinema models representing the geodetic branch for these faults with no dated offset features.

However, during the extensive review there were several cases noted in which either (a) there was a dated offset feature or dated overlap assemblage that was not included in the NeoKinema models or (b) that the NeoKinema prediction of slip rate had been biased upward by use of UCERF3 Fault Model FM3.1 and FM3.2 fault traces that are probably incomplete and therefore too short or (c) that NeoKinema had partitioned slip badly between two closely spaced parallel faults with no intervening GPS benchmarks.

We agreed at the fault-by-fault review meetings that it would be appropriate to manually adjust certain NeoKinema slip-rate predictions for use in UCERF3 hazard calculations. These

corrections just impose geologic rates or bounds, which would have been imposed before the computation if these data were available. Although a change in NeoKinema input data followed by a full recomputation would be more rigorously correct, there were two practical considerations: (1) There is no time to re-review secondary fallout changes in slip rates of neighboring faults that would be likely to occur in a recomputation and (2) maintaining perfect consistency between the fault-slip-rate and continuum-deformation fields of the NeoKinema models was not critical, because there were no current plans to use the latter in UCERF3. Similarly, there is no need to worry about locally incorrect continuum-deformation rates in a few small areas inside California when the model is used to estimate hazard of other western states in NSHM2014.

Adjustments

All of the following adjustments concern faults in California. They are referred to by their official names in UCERF3 Fault Model FM3.1 and/or FM3.2:

- **Bennett Valley**: This dextral fault is parallel to, and ~2–4 km northeast of, the dextral Rodgers Creek section of the longer Rodgers Creek-Healdsburg Fault. GPS indicates a total dextral slip of ~12 mm/yr on these two faults. However, it does not clearly dictate the allocation, because there are no benchmarks between the faults, and the regional GPS velocity field (in a 30×30 km square about them) shows only a smooth gradient, with increasing northwestward velocities to the southwest. NeoKinema put ~9 mm/yr on the Bennett Valley Fault because it is well aligned with the fast-slipping Maacama Fault to the northwest. However, putting only ~3 mm/yr on the Rodgers Creek did not honor the geologic constraint of 8.4±2 mm/yr (Schwartz and others, 1992). In this manual edit of the two models for UCERF3.3, ~5.7 mm/yr of dextral slip was transferred from the Bennett Valley Fault to the Rodgers Creek segment (minisection ID's 651.01~651.05) of the Rodgers Creek-Healdsburg Fault. This sets the Rodgers Creek rate to equal the geologic constraint and leaves ~4 mm/yr dextral slip on the Bennett Valley Fault, which has only qualitative (and somewhat ambiguous) geologic constraints.
- **Cady**: NeoKinema slip rates are reduced from 2.09 mm/yr (FM3.1) and 1.892 mm/yr (FM.32) to the geologic upper bound of 1.0 mm/yr. This bound is based on the report by Schmidt and others (2010): total sinistral offsets measured in outcrops and by aeromagnetic-anomaly correlation, plus a model age of ~10–6 Ma for the initiation of slip.
- **Calaveras (So)-Paicines extension 2011 CFM**: NeoKinema slip rates increased from 6.14 mm/yr (FM3.1) and 5.782 mm/yr (FM3.2) to 9 mm/yr, which is based on the Perkins and Sims (1988) and Bryant and Cluett (1999) reports that a terrace rise of age 13.9 ka is offset dextrally by 125 m.
- **Cleghorn**: NeoKinema slip rates decreased from 1.13 mm/yr (FM3.1) and 1.136 mm/yr (FM3.2) to the geologic upper bound of 0.6 mm/yr. R.J. Weldon, II (written commun., 2012) now interprets that terraces were miscorrelated in an earlier publication (Meisling, 1984), and assigns corrected ages.
- **Collayami**: NeoKinema slip rates decreased from 3.43 mm/yr (FM3.1) and 3.393 mm/yr (FM3.2) to the geologic upper bound of 1.0 mm/yr, based on Clark and others (1984), and Bryant (2000) reports that "a poorly constrained dextral displacement of 0-0.5 km for

the 0.5-0.6 Ma Thurston Creek rhyolite ... yields a minimum late and middle Quaternary dextral slip rate of 0 mm/yr and a maximum slip rate of about 1.0 mm/yr."

- **Hector Mine**: NeoKinema slip rates reduced from 5.43 mm/yr (FM3.1) and 5.528 mm/yr (FM3.2) to 2.533 mm/yr (FM3.1) and 2.671 mm/yr (FM3.2), which are the rates from the previous (UCERF3.1) NeoKinema models. Inferred slip rates on this fault are very sensitive to how post-earthquake (and perhaps pre-earthquake) transients are removed from the GPS velocity dataset. The UCERF3.1 GPS dataset was edited by Tom Herring, and the UCERF3.2/NSHM2014 GPS dataset was edited by Rob McCaffrey. Without implying any overall preference or judgment about these alternative versions, it seems prudent to take the lesser slip-rate estimate in this case where both "geodetic" (NeoKinema) rates are substantially higher than geologic estimates.
- **Lions Head 2011 CFM**: NeoKinema slip rates reduced from 0.930 mm/yr (FM3.1) and 1.143 mm/yr (FM3.2) to the geologic upper bound of 0.05 mm/yr, based on Clark and Slemmons (1990) reported rates constrained by the vertical throw of the crustal block between the Lions Head and Casmalia Faults.
- **Silver Creek**: NeoKinema slip rate reduced from 1.76 mm/yr in the FM3.1 model to the geologic upper bound of 0.2 mm/yr. This is based on seismic-reflection and well data (Wentworth and others, 2010) showing that several hundred meters of late Quaternary sediment overlie the fault trace and are only warped but not faulted. There is no need to adjust the NeoKinema slip rate of 0.057 mm/yr predicted in the FM3.2 version of the model, which is already below this bound.
- **Zayante-Vergeles 2011 CFM**: NeoKinema slip rate reduced from 2.86 mm/yr (FM3.1) and 1.366 mm/yr (FM3.2) to the geologic upper bound of 0.2 mm/yr, based on the Clark and others (1984) report of a late Quaternary net slip rate of between 0.03 and 1.4 mm/yr using data in Coppersmith (1979). The throw rate was correctly imposed, but a measured fault rake was overlooked in calculating those higher slip rates.
- **Dextral faults in western Joshua Tree National Park**: Eureka Peak, Burnt Mountain, and Joshua Tree: These three faults form a bundle of closely spaced, subparallel dextral faults in the Little San Bernardino Mountains in western Joshua Tree National Park. Their traces (which are the same in FM3.1 and FM3.2) are probably incomplete because they do not extend north to the Pinto Mountain Fault, or south to the San Andreas Fault. Strong geodetic constraints cause this region to shear at 8 mm/yr in both NeoKinema models of the long-term crustal velocity field. However, because of the incomplete fault traces, predicted slip rates were artificially increased to sums of ~17 mm/yr in both models. These slip rates have been scaled down by a factor of 0.464 in FM3.1 and 0.458 in FM3.2, so that they sum to the geodetic rate of 8 mm/yr. For this correction only, the continuum strain rates were also manually adjusted.
- **Contra Costa shear zone**: This zone was described by Brossy and others (2010) as follows: "The youthful East Bay hills structural domain contains a series of left-stepping, en echelon dextral faults and lineaments, collectively termed the 'Contra Costa Shear Zone' (CCSZ), that extend about 50 km from the Northern Calaveras fault to the West Napa fault …". There is considerable complexity and uncertainty in this zone with regard to how slip is transferred amongst the North Calaveras, West Napa, and Concord Faults (see, for example, Unruh and Kelson, 2002a,b; Kelson and others, 2004, 2005). During the February 13–14, 2013, fault-by-fault review of earthquake rate results and subsequent

review, it was determined that a maximum acceptable slip rate for the Contra Costa shear zone is 1.0 mm/yr (David Schwartz, oral commun., 2013).

It is recognized that the UCERF3 fault models oversimplify the Contra Costa shear zone, which allows geodetic deformation models to assign too much slip. We have therefore manually adjusted some fault sections (table C1) to reduce slip in the NeoKinema and Averaged Block models the least amount that will still allow their weighted average to sum up to no more than 1.0 mm/yr on the Contra Costa shear zone.

Block Models

Elastic Block Models

There were initially two different elastic block models among the UCERF3 deformation models. The "average block model" is a kinematically consistent average of five different block kinematic models. The "geologic block model" was an elastic block model with block-boundary slip rates bounded by the geologic slip rates. The geologic block model was dropped because the slip-rate constraints caused unacceptable rake variations, such as left-lateral slip on the San Andreras Fault, as a result of large off-fault strains that were required to satisfy the slip rate bounds. All of the block models used for the average block model are constrained by the same GPS and geologic data (figs. C1 and C2) and use the same block-boundary geometry (fig. C5). The methodologies, however, are different for each of the block models. Elastic block modeling has been used for years to infer fault slip rates from geodetic data (for example, Bennett and others, 1996; Prawirodirdjo and others, 1997; Souter, 1998; McClusky and others, 2001; Murray and Segall, 2001; McCaffrey, 2002, 2005; Meade and Hager, 2005).

Briefly, a block model is constructed by dividing the crust into numerous closed, fault-bounded blocks. The block geometry adopted for UCERF3 is shown in figure C5. It is not possible to incorporate all UCERF3 fault traces as block boundaries. The block boundaries were constructed with the help of Tim Dawson and Ray Weldon to follow the high-slip-rate, through-going faults in the UCERF3 fault database.The velocity field in all the block models is constructed as the sum of a long-term velocity field and a transient, interseismic perturbation to the velocity field due to backslip on fault boundaries. The contribution to the velocity field from backslip on faults is constructed using dislocations in a homogeneous elastic halfspace for all of the kinematic models. This deformation accounts for the elastic strain across faults due to interseismic locking. The long-term velocity field is constructed differently in the various kinematic models, which are described briefly below.

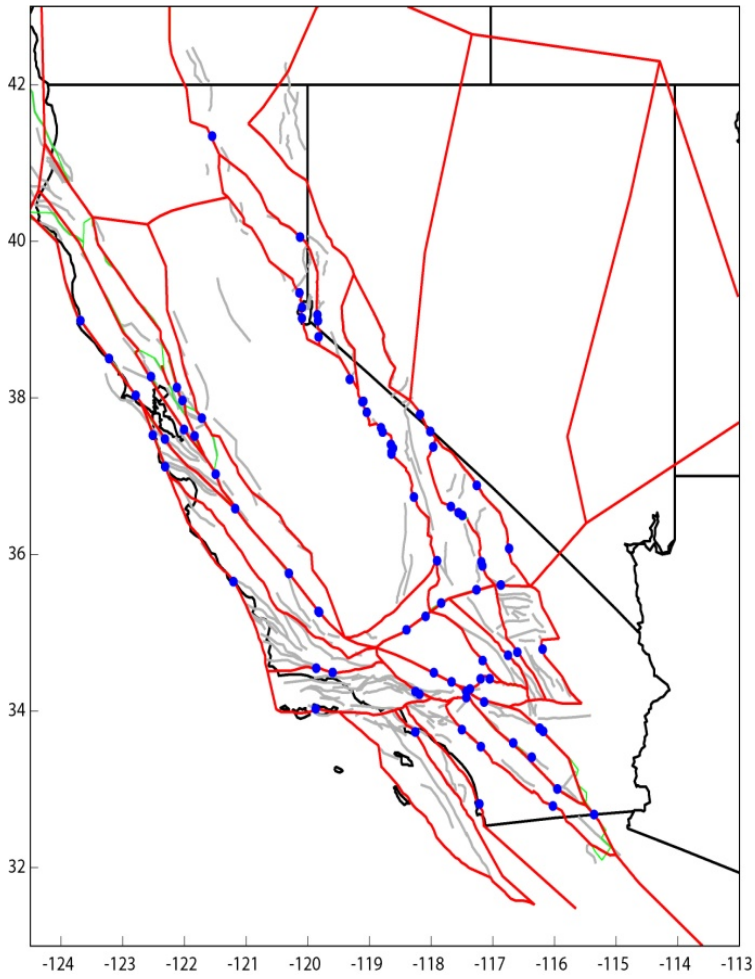

Figure C5. Map view of the UCERF3 fault traces (grey) and the block boundaries (red) used for the block-like model.

DefNode

DefNode is well documented in the literature. It was first described in McCaffrey (2002), with a few elaborations described in McCaffrey (2005). The Pacific–North American Plate boundary is represented as a series of rotating blocks separated by faults. The description of the motions of the blocks is mathematically identical to methods of estimating rotations of the large tectonic plates on the Earth's surface. A complexity in applying plate tectonic concepts directly to small regions, particularly when using short-term geodetic data, is that, in addition to rotations, increases in stress through time on the block-bounding faults result in elastic strain rates within the blocks. The strain rates cause surface velocities derived from GPS measurements to deviate from those expected from rotations alone and therefore do not comply with the "rigid plate" requirements of plate tectonics. In DefNode, the strain rates arising from such fault-stress changes are estimated simultaneously with the block motions using the "backslip" approach of Savage and Burford (1973) and the elastic half-space dislocation formulas of Okada (1985).

In addition to solving for block rotations and fault coupling, DefNode uses two additional types of parameters in the inversion: one to represent nonrecoverable, inelastic horizontal strain rates within the blocks and another to rotate published GPS-derived velocity fields into a common reference frame. The short-term strain rate within a block can comprise a recoverable (elastic) part due to stress changes on its bounding faults and a nonrecoverable (permanent) part that likely occurs by slip or localized strain on internal faults. In the long run, the elastic strain does not result in changes to the block's shape, whereas the permanent strain does; such behavior is often, but not uniquely, represented by an elastic-plastic rheology (for example, Turcotte and Schubert, 1982; Peltzer and Tapponnier, 1988). The inclusion of permanent strain rates within blocks is intended to represent more distributed deformation on faults at scales smaller than can be reasonably represented by blocks.

The long-term velocity field is described by a rigid-body motion of blocks plus a uniform strain-rate field (linear velocity field). The fault-normal and fault-parallel slip rates across boundaries are given by the velocity discontinuities at boundaries introduced by this long-term velocity field. As in all the kinematic models used for UCERF3, interseismic deformation due to locking of faults is introduced with backslip using dislocations in an elastic halfspace. Spatially variable backslip (coupling) on faults is estimated in the inversion.

Hammond Block Model

It is assumed that the surface motion can be approximated as piecewise continuous block rotations on a sphere and that at the boundaries of the blocks are in contact, locked at the surface but slipping continuously at depth (for example, Savage and Burford, 1973). This strategy (Hammond and others, 2011) for extending the concept to many blocks bounded by finite fault segments is similar to those of other recently introduced block modeling schemes (for example, Bennett and others, 1996; Prawirodirdjo and others, 1997; Soute*r*, 1998; McClusky and others*,* 2001; Murray and Segall*,* 2001; McCaffrey, 2002, 2005; Meade and Hager, 2005). GPS velocities are assumed to represent the interseismic velocity field, that is, they have been measured between large earthquakes, and the effects of nonsecular processes are either nonexistent or have been estimated and removed. Thus the long-term velocity (averaged over many seismic cycles) is equal to the sum of the interseismic and coseismic velocities, taking account of the predefined block geometries and fault dips. Thus, effectively, the only parameters that need to be free are the block rotations. To enforce this, an additional constraint that the relative motion of the blocks should be related to the slip rate at the fault is included. This constraint is equivalent to assuming that the horizontal long-term rate of relative motion across block boundaries is equal to the horizontal projection of the slip rate on the fault. The distinction is important because it is the basis for forcing the slip rate on the fault to be determined by all data on the block, not just data near the fault. Adding these constraints results in 2N + 2P equations that constrain 3M + 2P unknowns, where N is the number of GPS velocities, P the number of fault segments and M the number of blocks. This implements the backslip approach introduced by Savage and Burford (1973). In this context ‘‘coseismic velocity’’ is defined as the rate of movement of a point near the fault associated with coseismic offsets averaged over many seismic cycles. The slip rates are unknowns that scale the Greens functions representing the pattern of strike slip and normal slip for each fault segment. These Green’s functions are calculated for each fault segment using the functions of Okada (1985, 1992), because the dip, length, width, and depth of the fault are predefined.

Johnson Elastic Quasi-Block Model

This quasi-block model is described in Johnson and Fukuda (2010). It is described as a "quasi-block" model because it is not a block model in the same sense as other block models. The long-term velocity field is constructed in an elastic plate overlying a substrate providing buoyant gravitational restoring forces. The long-term velocity field far from block boundaries is described with a rigid-body motion plus a spatially variable strain-rate field parameterized with cubic polynomial basis functions. At fault boundaries, the fault-normal velocity discontinuities across faults are canceled with opening-mode dislocations in the elastic plate. The interseismic velocity field is constructed by adding the contribution from locking on faults using dislocations in an elastic halfspace, as in all other elastic block models. Creep below the locking depth is assumed to occur at zero stressing rate (approximately). Locking depths are fixed at 15 km for all inversions. Faults with known surface creep are assumed to creep at the long-term slip rate from the surface to a depth of 5 km. For fixed locking depths, the inversion for slip rates and off-fault strain rates is linear and uses least squares formulas.

Average Block Model

The "average block model" (ABM) is a kinematically consistent average of five different block kinematic models. All five of these block models adopted the same GPS and geologic data (figs. C1 and C2) and the same block-boundary geometry (fig. C5). The five block models include the three traditional elastic block models (Hammond, DefNode, and Johnson) and implementations of the Zeng-Shen model and NeoKinema using the block geometry (note that these two models are not the same as the faulted continuum, non-block models that are under consideration as alternative UCERF3 deformation models).

We combine the results of these five block models into a single average model, called the "average block model." This averaging is done in a kinematically consistent way by using the model slip-rate estimates from all five inversions as "data" in a unified block model inversion. The GPS data are also used as constraints to stabilize the inversion for the block strain rates, but the GPS data are down-weighted relative to the slip-rate constraints by a factor of 10.

The block model used for this averaging inversion is a modified version of the Johnson quasi-block model formulation. For this calculation we do not compute the long-term velocity field in an elastic plate as in the published version of the Johnson block model, but rather we adopt an approach that is similar to traditional block models. The general method is illustrated in figure C6. As in traditional block models, the long-term velocity field is represented as the sum of a rigid body motion (fig. C6b) and spatially variable strain rates (fig. C6c) parameterized in this case with cubic polynomials. Because these two contributions to the velocity field introduce fault-normal velocity discontinuities across vertical faults, and because UCERF3 does not allow this component of motion on faults, we distribute this discontinuity into long-term distributed off-fault strain by cancelling the velocity discontinuity above the locking depth with opening mode dislocations (note that this is entirely consistent with the traditional block model approach, but although this fault-normal slip component of strain is traditionally interpreted as elastic, recoverable strain, we have mapped this into the long-term off-fault strain for UCERF3). This cancellation step is illustrated in figure C6e. Also, because some of the block boundaries do not have corresponding UCERF3 fault traces (there are places where discontinuous UCERF3 fault traces were connected to form contiguous block boundaries), we distribute the modeled slip on these phantom fault segments into permanent off-fault block strain by canceling the fault-parallel

slip rate above the locking depth using elastic dislocations (fig. C6f). This is similar to the approach for removing fault-normal velocity discontinuities.

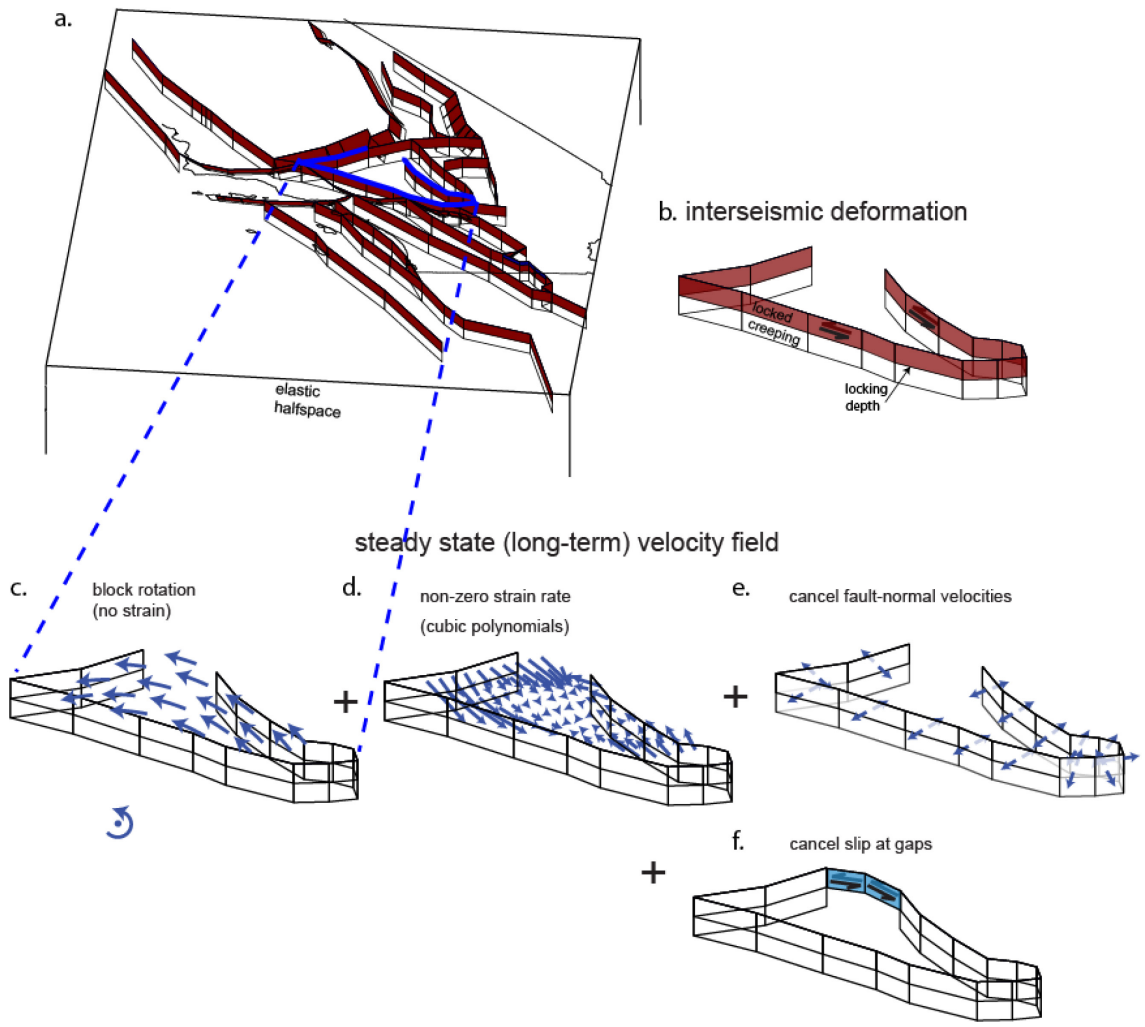

Figure C6. Diagrams illustrating the block model formulation used to construct the average block model and the geologic block model. *a*. Typical block boundary construction (not same as UCERF3 geometry). *b*. Backslip is imposed above locking depth. *c-f.* Components of long-term velocity field. See text for details.

The interseismic velocity field is computed, as in all block models, by adding the contribution from backslip on locked faults using dislocations in an elastic halfspace. For this work we have assumed a uniform 15-km locking depth for all of the faults. For fault segments that display significant shallow creep, we assume creep at the long-term slip rate down to a depth of 5 km (or 15 km, that is, no coupling, for the central San Andreas creeping section).

The final step in the block modeling is to compute slip rates on faults that are not on block boundaries (the gray traces in fig. C5). Here we describe two different approaches that we examined for UCERF3 (methods A and B). Method B was chosen for the final average block model submitted for UCERF3.

Method A. In this approach slip rates on off-block boundary faults are calculated by integrating the long-term block strain rates across faults. We do this by integrating half of the strain within a 10-km swath (5 km on each side) along lines perpendicular to the fault sections. From this we compute the fault-parallel and fault-normal velocity difference across the fault, which we interpret as fault slip rate. Half of the strain remains as off-fault strain.

Method B. In this alternative approach we do not solve for parameterized block strain rates (the cubic polynomial terms illustrate in fig. C6d). The only contribution to off-fault strain rates comes from the "cancelation" of fault-normal velocity discontinuities and gaps, as illustrated in figure C6e,f. Off-block-boundary fault segments are represented with dislocations buried at 12-km depth (steady creep imposed on dislocations extending from 12 km to infinite depth). This is the approach adopted in the Zeng-Shen model for all fault sections. We simultaneously solve for the block rotation rates (giving block boundary slip rates) and the buried dislocation rates. An initial value is placed on the rate and rake for each off-block-boundary fault. The initial values originate from a truncated Gaussian distribution with mean equal to the geologic model rate, standard deviation equal to a quarter of the width of the geologic bounds (from the upper and lower limits in the geologic model) and truncated at the geologic bounds (zero probability of slip rate outside of geologic bounds). This is formulated as a constrained least-squares inversion with strict upper and lower bounds (inequality constraints) on the off-block-boundary faults.

Method B was chosen for the final average block model (ABM). Method A produced slip on off-block-boundary faults that varied wildly in rate and rake along strike. The style of slip was inconsistent with the expected style from geology in numerous locations. Furthermore, the internal block strain rates in Method A lead to some sizable along-strike gradients in slip rate on block boundaries, most notably the creeping section and the north coast sections of the San Andreas Fault. Method B removed these problems noted in Method A.

Figure C7 illustrates the results of using Methods A and B in the Transverse Ranges region of southern California. Method A is referred to as "Integtrated block strain rate" and Method B is labeled "Buried dislocation." The strain rates from Method A are shown, along with the slip rates and rakes for both methods. The figure illustrates how much of the along-strike gradients in rake and slip rate that are clear in Method A disappear in Method B. By design, the rakes and rates in Method B are consistent with the geologic model, whereas there are a number of faults in Method A that have rakes that are inconsistent with geology.

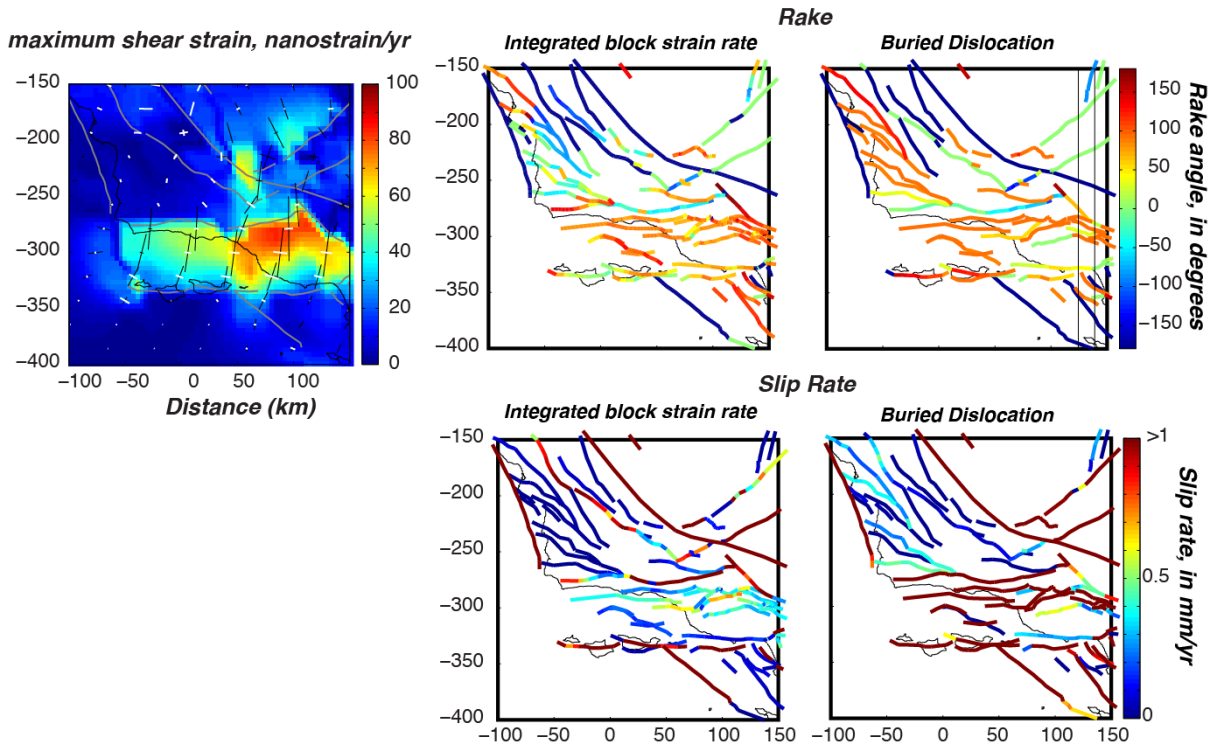

Figure C7. Maps comparing estimated slip rates and rakes in the Transverse Ranges region of California using Method A (integrated block strain rate) and Method B (buried dislocation). The maximum shear strain rate is shown for Method A. These strain rates are integrated to obtain the slip rates and rakes in Method A. Note large along-strike gradients in slip rate and rake in Method A, but not in Method B. Some of the rakes in Method A are inconsistent with the geologic model, especially north of the Transverse Ranges in the Santa Maria and surrounding basins.

Manual Edits to the Average Block Model

An unacceptably high change in hazard was noted in trial runs of the UCERF3 methodology in northwest California (fig. C8), which was traced back to a high slip rate on the Big Lagoon Fault in one of the four deformation models, the ABM. During the February 13–14, 2013, fault-by-fault review of earthquake rate results, a consensus conclusion was reached that the modeled slip rate on the Big Lagoon by ABM was too far out of range on the basis of geological evidence. The ABM has slip rates on this fault as high as 9.6 mm/yr, whereas the maximum rate from geology is 1.2 mm/yr. The other three models have mean slip rates very close to 1 mm/yr.

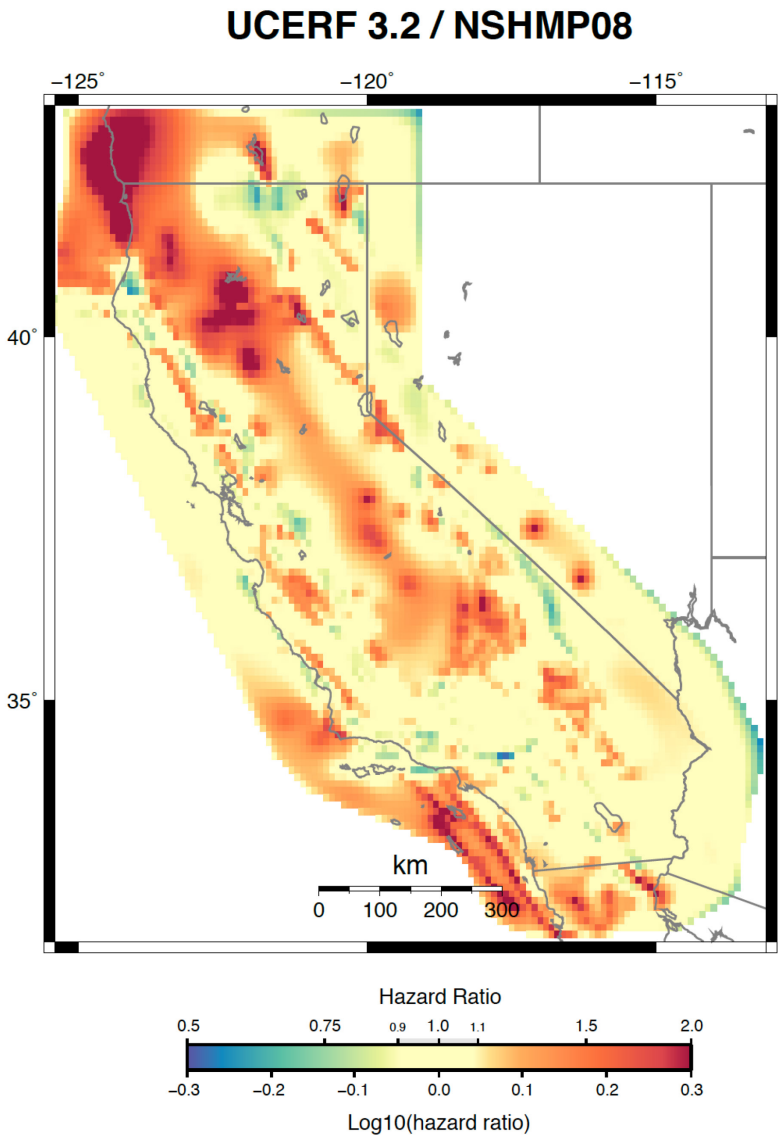

Figure C8. Map showing ratio of calculated hazard from UCERF3.2 to that from the National Seismic Hazard Map Program version of 2008 (NSHMP08); red shaded areas thus show hazard increases relative to NSHMP08, and blue areas indicate reductions. The increase in hazard in northwest California was caused by excessive slip rate placed on the Big Lagoon Fault on a block boundary in the average block model.

Because of the nature of their construction, we note a general tendency of block-style models to have high slip rates along block boundaries. The success of this approach depends on the actual degree of block-like behavior observed in the earth, which can vary spatially. The Big Lagoon Fault is part of the northernmost block boundary of the ABM, and therefore has more a role as a boundary condition than as a fully defined block with a complete inventory of faults internal to the block. We therefore propose to reduce the ABM slip rate on the Big Lagoon Fault to 1 mm/yr. This change does not produce a covariant affect on other faults in the ABM because it lies on the northernmost boundary of the model. None of the UCERF3 deformation models

fully describe relative plate motions at this latitude, which is superseded by the NSHMP Cascadia model.

A Fault-Based Model for Crustal Deformation in California (Zeng and Shen Model)

Overview

In this model formulation (Zeng and Shen, submitted), block boundaries are represented as buried dislocations in a homogeneous elastic half-space. Each fault segment slips at a solved-for slip rate beneath a locking depth, except at a few fault segments where shallow creep is allowed. Slip-vector continuity at fault nodes or intersections is imposed to regulate slip variability and to simulate block-like motion. In addition, fault-normal slip rates are minimized because fault systems in California are dominated by strike slip faults. The slip distribution is estimated using a least-squares inversion. An increase in the weighting of the continuity constraint will result in a more block-like deformation model. A very loose conservation constraint results in a fault-patch-only deformation model. The degree of weighting on the conservation constraint is optimally selected from a trade-off curve between the data postfit residual chi-squares and the parameter resolution of the model, so that certain nonblock-like deformation features are allowed, such as permanent or transient strain build up within bounding blocks. The locking depth is fixed to the values specified by the UCERF3 fault model.

This model formulation assumes zero slip rate on all faults as an initial condition and applies geologic constraints at the points where they were measured. The exception to this is on some minor faults where significant departures from faults with well-constrained geologic data were encountered. In these instances constraints are imposed on all the fault subsections.

Two separate models are developed for UCERF3: a block-like model and a fault-based model for California. Slip-rate parameters from our block-like model, one of the five block-like models, will be used to develop the average block model (discussed in a previous section), which finds a kinematic consistent average from all five model inputs. Our fault-based model provides slip-rate estimates on UCERF3 faults based on GPS observations and geologic slip-rate estimates at more than 100 points. The fault-based model also provides gridded off-fault strain rates to compare with other seismic hazard inputs—that is, the Gutenberg-Richter a-value distribution based on seismicity, regional strain mechanisms as determined from earthquake moment tensors and focal mechanisms, and earthquake moment budget from other studies.

Method

Zeng and Shen (2012) developed a kinematic fault network model that simulates geodetic surface deformation rates from a given distribution of slip rates across all the faults in the region. For a given slip-rate and creep rate distribution on faults, the ground velocity vector at any point is obtained by taking a spatial convolution of the static point source Green's function with the slip rate functions over the faults:

$$\dot{u}(r_i) = \sum_{j=1}^{N} \left(U^1_{nj} \Delta \dot{u}^j_1 + U^2_{nj} \Delta \dot{u}^j_2 \right) + \sum_{k=1}^{M} \left(U^1_{creep,nk} \Delta c^k_1 + U^2_{creep,nk} \Delta c^k_2 \right) \quad (5)$$

where $\dot{u}_n$ is the predicted surface velocities, and n is the component of the velocity. Here we only consider the two horizontal components: $\boldsymbol{r}_i$ is the location of the i-th station, $\Delta\dot{u}_1^j$ and $\Delta\dot{u}_2^j$ are the fault-parallel and fault-normal slip rates along the j-th fault segment, respectively. U_{nj}^1 and U_{nj}^2 are the Green's function relating those fault slip rates to velocities at the i-th station; Δc_1^k and Δc_2^k are the fault-parallel and fault-normal creep rates along the k-th fault segment, respectively; and $U_{creep,nk}^1$ and $U_{creep,nk}^2$ are the Green's function relating the fault creep rates at shallow depth to velocities at the i-th station. N is the total number of fault segments, and M is the total number of creeping fault segments.

Our kinematic fault model assumes that each fault segment slips at a certain rate beneath a locking depth, except at a few fault segments where shallow creep is allowed. We also impose slip-vector continuity at fault nodes or intersections to regulate slip variability and to simulate block-like motion. In addition, we minimize slip rates along the fault-normal direction because fault systems in the region are dominated by strike slip faults. Together with equation 5, they form the basis for solving for the slip distribution using a least-squares inversion. We use Okada's formulation and code (1992) to calculate the surface deformation in a elastic half-space.

GPS Data

We use the GPS data discussed in the section on data above. There are reported uncertainties in the velocity field that are as small as 0.03 mm/yr. Our test inversions find that these extremely small uncertainties can overweight these observations, so a lower cutoff of 0.2 mm/yr was used to avoid excessively overweighting during the inversions. In addition, the velocity field has also been carefully edited by Rob McCaffrey using visual inspection of the velocities for their consistency with neighbors and for residuals relative to the model. To avoid these edits being model dependent, data are only removed where their residuals are not consistent with neighbors, at the 3–4 mm/yr level, and also if they are not near faults. Some USGS campaign GPS data from near the Yucca Mountain region have rates that are different from the azimuth of the rates from the continuous stations in the area. They are also different from what are reported on the USGS GPS website. The difference might be introduced during the rotation combination of those velocity fields into the rest of the other GPS velocities. Those data were removed on the basis of Bill Hammond's and Peter Bird's recommendations. Peter Bird also contributed to removing some additional outliers in the velocity field. We also removed data with sigma larger than 1.0 mm/yr.

Geologic Data

The geologic slip-rate file is a compilation of Quaternary geologic slip rates for faults in the UCERF3 fault model (appendix B, this report). Instead of the expert opinion or consensus slip rates adopted by UCERF2, this compilation is intended to be a purely geologic estimate of late Quaternary slip rates at locations along faults within the UCERF3 fault model. This compilation does not include slip rates that rely on assumptions of characteristic slip, are heavily model dependent (such as using assumptions of horizontal to vertical slip to derive horizontal slip rates from amounts of vertical offset), or that are in need of revision because of revised dating at a site. Rates that are somewhat suspect, because they may be derived from features offset by a limited number of earthquakes that may not represent a longer term average are also

excluded. A single representative slip rate or averaged slip rate is reported for any location. The compilation also includes selected entries from an extensive database of slip rates (including long-term rates) that Peter Bird (UCLA) has compiled using the same criteria described above. We use either the preferred rates or averages of the minimum and maximum values as our geologic constraints with their corresponding uncertainties. For some sites, uncertainties are not available. We compute a linear regression between slip rates and their standard errors (fig. C9) and assign the predicted uncertainties from this regression to the rates at those sites. We only consider sites that are located along the block boundaries for the block-like model, or along the UCERF3 fault traces for the fault-based model. Figure C2 shows the geologic sites used for the fault-based model.

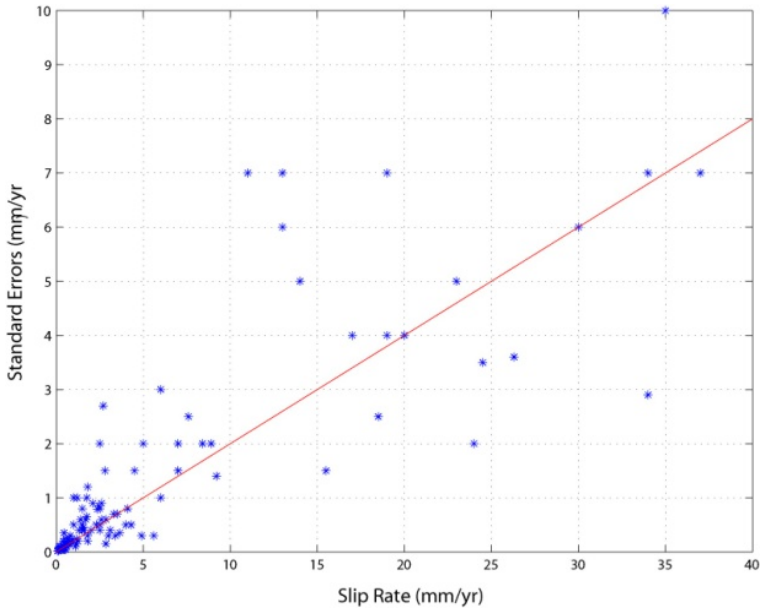

Figure C9. Graph of geologic slip rates versus their standard errors determined from the table provided by Tim Dawson. Red line is the linear fit to the data and is used to predict standard errors for sites with only slip-rate information available.

Fault Model

For the fault-based model, we use the UCERF3 dip angles and locking depths. We also added a few Nevada faults near the Reno-Carson City area. Figure C2 shows fault traces of our fault-based model. We impose a slip-vector continuity condition for the major faults in the region so that the zones enclosed by those faults will behave more block-like. We also added a southern branch to extend the San Andreas Fault system into Mexico and northern branches to extend the northern San Andreas and Cascadia Faults farther east and north of the triple junction, respectively. Again, these additions allow us to better model the far-field relative motions between the North American Plate and the Pacific Plate.

We have introduced shallow creep in some of the fault segments—for example, along the central California creeping segment of the San Andreas Fault, Calaveras Fault, Hayward Fault, Imperial Valley Fault, Brawley seismic zone, and others. We also allow partial locking for the northern Parkfield and southern Santa Cruz Mountains segments of the San Andreas. The depths of the creeping segments are set at 10 km for most creeping faults, except for the central California creeping segment and the Brawley seismic zone. In the central California creeping zone, we have set the creep rates as a function of depth. The creeping depth along the Brawley seismic zone is set to be equal to its locking depth because of its shallow seismogenic zone. The amount of creep along those segments is determined from inversion of the GPS observations.

Zeng-Shen Model Results and Discussion

We compute inverse solutions for both block-like and fault-based deformation models and use the same weighting parameters for the slip-rate vector continuity constraints across fault node points and for minimizing slip rate along fault normal component as in Zeng and Shen (2012). In additional to the geologic constraints on slip rates at locations where geologic estimates are available, we also imposed a 50-mm/yr rate at the southern and northern ends of the San Andreas Fault, and a 10-mm/yr subduction rate for Cascadia. For the fault-based slip-rate estimates, we imposed a partial fault-style constraint on some selected faults to avoid rake reversals. Figure C10 compares observed GPS velocities with the residual GPS velocities based on the fault-based deformation modeling. Those residuals are given by the differences between the observed velocities and model predictions, with a mean value of 1.6 mm/yr. The relatively large misfits in the Landers/Hector Mines area likely are artifacts of the long-term postseismic modeling conducted during data processing. Large misfits near the Long Valley Caldera area are partly caused by the Long Valley volcanism, which is not included in our model. Overall, we do not observe any systematic trend in the residuals that might suggest model bias. The model accommodates all of the major features observed in the GPS velocity field. In comparison with figure C4, the current model based on inversion of geodetic and geologic data constitutes a significant improvement over the UCERF2 models based on expert opinions. Residual GPS velocity distribution for the block-like model is very similar to that of the fault-based model shown in figure C10b.

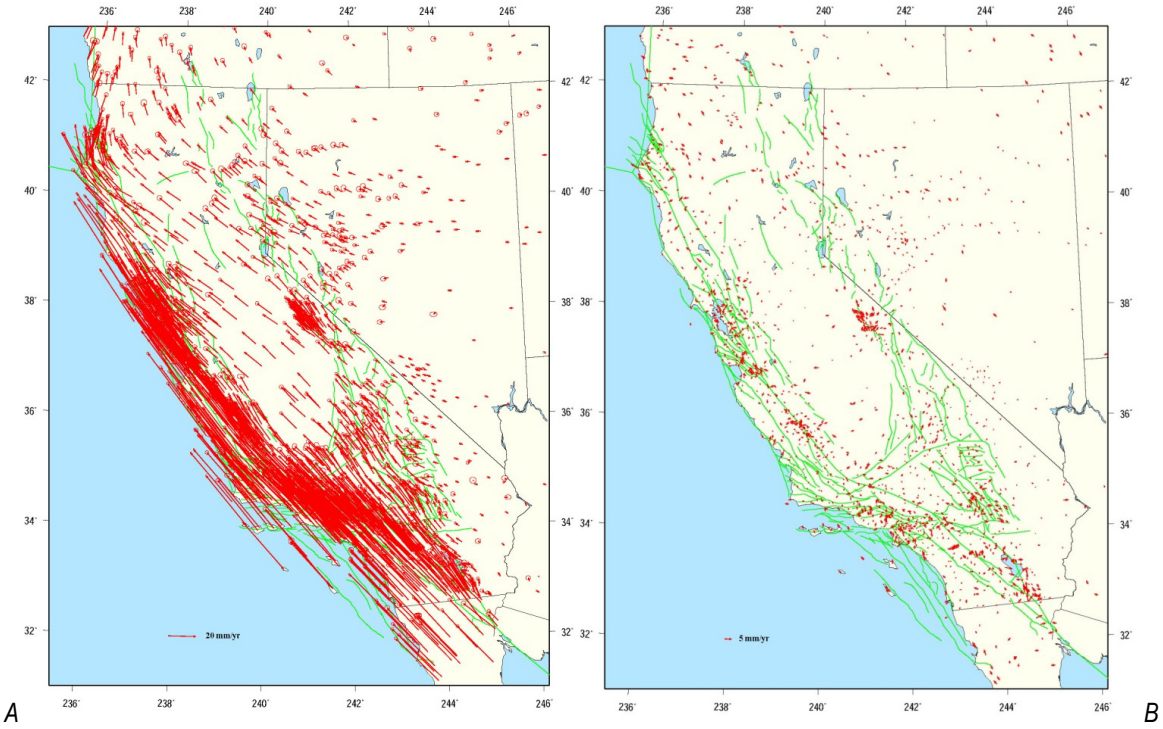

Figure C10. Maps showing observed and residual GPS velocities. (*A*) Distribution of GPS velocity vectors for California and its neighbors, referenced to the North American Plate. (*B*) Residual velocities for inversion using fault-based model with geologic constraints. The green lines are the modeled fault traces. The residual vectors are plotted at the same scale as the GPS velocities in (*A*).

In comparison with the UCERF3 geologic slip-rate data and the geologic bound data, slip rates from Santa Cruz all the way to the north coast and offshore segments of the San Andreas Fault agree well with the geologic estimates. Slip rates also agree well with the geologic observations along the Calaveras-Hayward-Maacama Fault segments and the Greenville-Great Valley Fault segments in the north, and along the Central Garlock and San Jacinto segments in the south. In contrast to previous studies (for example, Meade and Hager, 2005; McCaffrey, 2005), slip rates found along the Garlock Fault agree closely with the geologic rates. Slip rates along the Coachella Valley and Brawley segment of the San Andreas Fault are nearly twice the rates along the San Jacinto Fault branch. For offshore faults, slip rates are within the geologic limits but near the lower bounds for fault segments along San Gregorio, Hosgri, Catalina, and San Clemente Faults. Although the slip rates along the Bartlett Springs Fault are 2–3 mm/yr above the geologic bound, the total slip rates across various transects of the northern San Andreas Fault, Calaveras-Hayward-Maacama system, and Bartlett Springs-Greenville-Great Valley Faults are around 40 mm/yr, matching the regional tectonic rates.

Discrepancies between geologic and geodetic estimates on fault slip rates will provide us insight into the complex interactions in the system, or the extent of incompleteness of our deformation model. Figure C11 plots GPS-based slip rates against the geologic slip rates. The GPS-based slip rates are obtained from inversions with the fault-based model and geologic constraints. The geologic slip rates are obtained from the UCERF3 slip-rate data file.

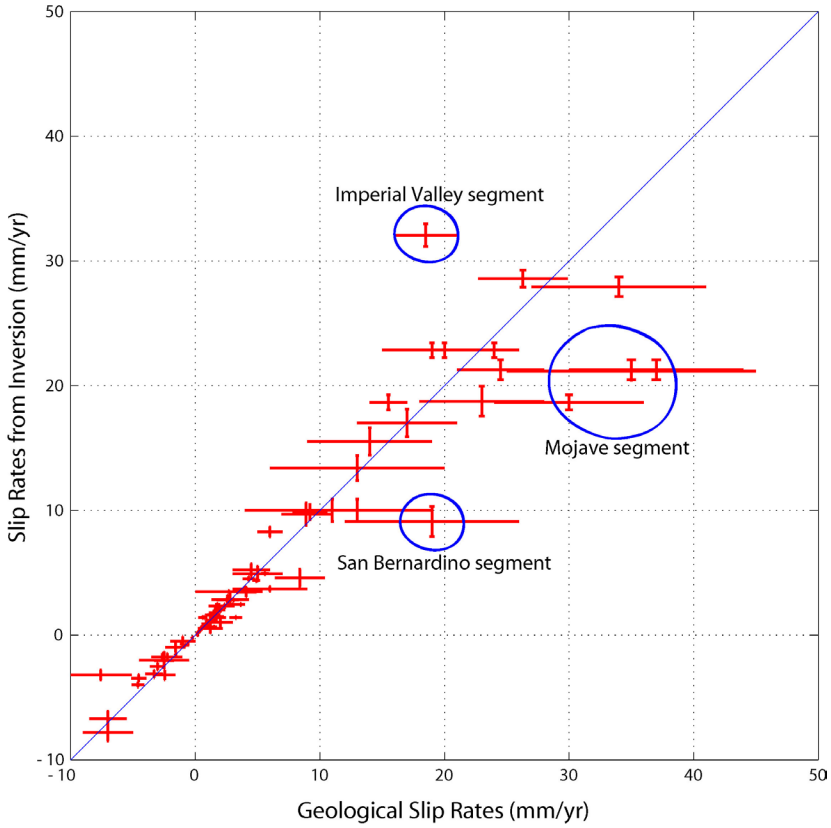

Figure C11. Graph of GPS slip rates versus geologic slip rates for California faults. The GPS slip rates are calculated by inversion with the fault-based model and geologic slip-rate constraints. The geologic slip rates are from Tim Dawson's slip-rate data based on pure geologic observations. Outlier values are circled from the Mojave and San Bernardino segments of the San Andreas Fault.

GPS rates are higher than geologic slip rates mostly on faults in the Eastern California Shear Zone and Walker Lane. GPS rates are lower than geologic slip rates mostly along the central and southern San Andreas, particularly along the Mojave, San Bernardino Mountain and San Gorgonio Pass segments. Despite the discrepancy, correlation between the geologic estimates and the GPS solutions are high, with a correlation coefficient of 0.9. Statistically this indicates a strong linear dependence between the GPS estimates and the geologic estimates, suggesting that the geodetic and geologic data are highly compatible for the region.

Zeng-Shen Model Updates

An exploration of tradeoffs between fitting geodetic and geologic data was carried out using the Zeng-Shen model. The questions addressed were: how large do the GPS data residual misfits get if all faults, or just all type B faults, are constrained to have slip rates within geologically defined bounds? For background, type A faults are defined in the National Seismic Hazard Map parlance as those that have high slip-rates and sufficient data on timing of past events and slip-per-event that detailed models of fault-zone behavior can be constructed. Type B faults are major faults with measurable slip rates but inadequate information on segmentation, displacement, or date of last earthquake

For both fault models (FM3.1, FM3.2) with all slip rates held within the geologic bounds, their normalized χ^2 errors are 18.40 and 18.44, respectively. When only B-fault slip rates are held within the geologic bounds, their normalized χ^2 errors are 15.10 and 15.16, respectively. For all tests, slip rates are not constrained within the provided geologic bounds for the Cerro Prieto and Imperial Faults because the best-fit GPS rates for those two faults are in better agreement with the overall plate rate budget. A variable rate was retained for all mini sections in the central California creeping section. The average rate for the creeping section is within the provided geologic bounds. The bounds on the San Jacinto (Stepovers Combined) Fault for FM3.1 were set between 11.0 and 18.0 mm/yr to maintain consistency with the FM3.2 geologic bounds model.

We give weight to the Zeng-Shen B-faults model, which provides comparable GPS fits to other geodetic models. The Zeng-Shen all-faults constrained model is a useful exercise in understanding data tradeoffs, but not substantially different enough from the geologic model to warrant a new logic-tree branch.

Deformation Model Results

We compare and evaluate results from five deformation models. These models are the UCERF2 deformation model (Field and others, 2009) and four new models for UCERF3 (presented in detail in previous sections of this appendix). The UCERF2 deformation model was constructed primarily using geologically observed slip rates, but those rates were modified to be more consistent with geodetic data when necessary. An example of this is the Mojave section of the San Andreas Fault, where geologic interpretations favor a slip rate of 35 mm/yr, but geodetic models favor values closer to 20 mm/yr. UCERF2 adopted values of 27 and 29 mm/yr in its two deformation models to be within the error bounds of both geologic and geodetic data. Geodetic models of critical areas, such as the Meade and Hagar (2005) block model of the area around the San Gorgonio Pass, also strongly influenced slip rates of faults in those areas. The resulting model was checked against geodetically determined plate boundary motion, and zones of distributed deformation ("C-zones," areas of diffuse deformation of which 50 percent is presumed seismogenic) were added where geodetically measured deformation could not be accommodated on known faults.

The four new UCERF3 models are formally constrained by GPS observations and an updated database of geologically observed fault slip rates (figs. C1 and C2). All models thus match the primary observed data; the models are more heavily weighted toward the geologic observations at the points where high-quality measurements exist and near those locations (fig. C2), and they are not as tightly fit to the GPS field. The geologic model is constrained by slip-rate determinations from figure C2 and constraints described in appendix B (this report). Geodetic data were deliberately excluded from the geologic model to avoid the problem of the current geodetic models being constrained by previous rates that were influenced by geodetic data (like UCERF2 rates). Geodetic models all use the geologic slip-rate data shown in figure C2 as constraints. All fit the GPS data as described below, and the Zeng-Shen model as implemented for UCERF3 also includes the ranges of slip rates from the geologic model as constraints. NeoKinema and the Zeng model have faults as boundaries within a deforming region (faulted continuum models), in contrast to the average block model, which is composed of translating blocks and the internal strain within those blocks. All models are sensitive to the geometry of the faults included, and block models are particularly sensitive to the faults that are incorporated into block boundaries.

Our task then is to compare, contrast, and assess the seismogenic deformation solutions with a goal of deciding which models should be used for earthquake forecasting. Because all models are already fit to primary observations, we are left with examining them from secondary criteria and (or) expert opinion. We are thus looking for outliers to the general solutions that might influence hazard or that are violations of other data. If no deformation models are rejected, then they can be viewed as establishing a range of possible solutions. In that event, our task is to give the different solutions weighting factors for the UCERF3 logic tree if there is reason not to treat them equally. In this section we present and discuss the model outputs in as many different forms as we can. In a later section on model weighting we present initial weighting schemes for comment/revision/discussion purposes.

Notes on Relative Data Weights, Resolution, and Parameter Sensitivity

Details about data handling and parameters are given in the individual model description sections (and in appendix B, Dawson and Weldon, 2013). However some universal points about how different data are handled, and the implications of UCERF3 assumptions are important to keep in mind as the model results are presented and compared in the subsequent sections of this report.

Philosophy and Implications of Relative Data Constraints

As will be discussed in detail in subsequent sections, most of the geologic slip-rate estimates agree with those modeled using GPS data. This agreement between two very different estimation methods is encouraging, because in the UCERF3 GPS-model-based inversions, the geology is a loose constraint in most parts of California. This result is seen in other worldwide GPS-geologic comparisons that were made truly independently (for example see fig. C9; Thatcher, 2009). Because past WGCEP/UCERF efforts have always relied primarily on geologic slip-rate information to drive earthquake rate models, for UCERF3 we chose to include geologic rates as constraints; however, at least for the major faults, results would not differ significantly if this constraint were removed.

The disagreements between geology and geodesy, of which there are several notable ones in California (see section on slip-rate characterizations, below), are perhaps equally important. First they show, for example, that there is independent content in the GPS estimates. GPS rates are also important because geologic rates, although rightly the standard for comparison, are also estimates with their own individual strengths and limitations, not immutable constants of nature. So the two different datasets complement each other, providing what we would not otherwise have, an (albeit imperfect) estimate of the true range of possible slip rates on individual faults. Furthermore, the differences likely capture instances in which one or the other estimate has a systematic bias, either from unknown data error or temporal rate difference.

As discussed in the following section, UCERF3 deformation models fit GPS data to normalized χ^2 values ranging between ~5 and ~15, whereas inversions less weighted toward geologic constraints would want to try to fit data at the level between 3 and 4 (in an ideal world). It has been necessary in UCERF3 to seriously compromise the fit to GPS (and to misfit it systematically in some regions like the Mojave Desert) in order to honor the best geologic constraints. As discussed in detail in appendix B (this report) by Dawson and Weldon, slip rates off the major faults, either geologic or geodetic, are individually quite uncertain. Only about half of the geologic model rates are based on dated offset features, and ~4 dated offset features are required (Bird, 2007) to have a 50-percent chance of obtaining a well-constrained rate on each

fault. Conversely, many of these faults slip at <1 mm/yr and are individually blind to geodesy. Integrated displacement rates across several of these faults may locally be within the range of geodetic detection (for example, in the Ventura Basin or Eastern Mojave). Geologic slip-rate estimates for many of these faults are approximate, based on the time of the most recent major slip event. Dawson and others (appendix B, this report) suggest that, on average, these geologic estimates are likely correct within a factor of two or so, but individually they could be farther off.

There may eventually be better ways of estimating values for most of these low-slip-rate faults, but neither geologic nor geodetic approaches yield perfect estimates. The results are extremely sensitive to model assumptions (like a priori geologic constraints) and the difficulty of measuring rates on closely spaced faults and ones with low slip rates. Where available, the highest quality geologic estimates are likely superior because they do not suffer from these limitations.

Parameters and Uncertainty

The Savage and Burford (1973) model of elastic strain accumulation, which assumes a locked upper crustal fault underlain by a freely sliding fault at long-term slip rate, is a central assumption of all the UCERF3 geodetic models. Evidence in favor of this idea comes from major faults, where the GPS (or InSAR-derived) velocity profile perpendicular to vertical strike-slip faults in California, Turkey, New Zealand, and elsewhere looks like the expected arctangent function, and the slip rate predicted from this model agrees acceptably with geologic estimates (Thatcher, 2009, and references contained therein). In addition, mapping of tremor events on the Parkfield and Carrizo sections of the San Andreas Fault show unambiguously that a narrow shear zone extends beneath the surface trace down to the Moho or deeper (for example, Shelly and Hardebeck, 2010; Ryberg and others, 2010; Shelly and Johnson, 2011). Repeated shallow seismogenic slip on such faults creates a stress concentration beneath, and strain weakening and consequent localized deformation of a semibrittle or ductile material will eventually occur. This is supported both by laboratory deformation studies at appropriate temperature, pressure, and state conditions and stress or displacement-driven models of long-term steady-state slip or ductile flow. However, the Savage and Burford (1973) model was not necessarily intended for some dipping, low-slip-rate, and (or) low-cumulative-offset faults that may exist solely as accommodating structures adjacent to bends or other irregularities on major fault lines. Fault interaction may in part explain activity on these faults. Therefore a worthy goal for future forecasts would be to introduce more physics-based faulting models that are constrained by geology and GPS and that can model stress transfer between interacting fault structures.

Another free parameter involved in deformation modeling is the locking depth of faults. Because this is rarely well constrained by geodesy alone, it follows that the model results are not sensitive to modest changes in assumed locking depth. The UCERF3 geodetic models follow the earthquake-rate model assumptions of assigning locking depth to the maximum depth of seismicity, which is a proxy for the local brittle-ductile transition and hence the locking depth.

Ideally, uncertainties and covariance between model outputs could be reported for each geodetic model. Unfortunately these are difficult to provide because the computations are iterated and nonlinear. We could theoretically provide uncertainties and covariance from extensive Monte-Carlo testing of variations in the modeling parameters and input values, but this would require new programming, supercomputer resources, and 6–12 months of researcher time. The UCERF3 project plan recognized the scale of this problem from its outset, and the intended

approximation for this exercise was designed by securing multiple approaches to slip-rate determination as represented by the different deformation models discussed in this report.

Model Fits to GPS Observations

We present two measures of model fits to GPS observations: (1) normalized χ^2 values and (2) maps of residual velocities. A χ^2 test is the weighted sum of the residuals as

$$\chi^2 = \sum \frac{(obs - calc)^2}{\sigma^2}$$

where σ^2 is the variance on observations (taken to be ≥0.2 mm/yr. Reduced χ^2 is just divided by the number of degrees of freedom. Enforcing a close fit (χ^2 ~1) to the dense GPS field would result in slip-rate models with strong spatially varying values that might be overly influenced by localized variations in GPS measurements. A more relaxed fit captures the smoother, more regional nature of the geodetic observations. We provide normalized rather than reduced χ^2 here because values are divided by the number of observations rather than the degrees of freedom. Normalized χ^2 values for the three geodetic models range around 5.3 for NeoKinema, 15.1 for the Zeng-Shen model, and 15.9 for the average block model. These are on the higher side of typical levels of fitting for tectonic-scale models with a large number of observations (for example, Hsu and others, 2012), and result from giving geologic observations high weight in the inversions for slip rate. Mismatches between geology and geodesy are discussed for individual fault zones in a later section.

We show maps of the spatial distribution of mismatch between models and observed GPS in figure C12 and note a few features. The average block model does not seem to be capturing all of the right-lateral plate motion across the north coast region, because it has large southeast-directed residuals in that region. The NeoKinema model residuals point to excess right-lateral motion across the Mojave segment of the San Andreas Fault. The Zeng-Shen model does not seem to be capturing all of the Pacific-North American Plate motion, showing a systematic ~5 mm/yr southeast residual motion (meaning a right-lateral sense across California) in the Great Basin region of Nevada. There may also be insufficient contraction across the Transverse Ranges. Residuals in populated regions of southern California and the San Francisco Bay area are smallest in the NeoKinema model and next smallest in the average block model, with the largest being in the Zeng-Shen model (fig. C12).

Implied Seismic Moment Rates

UCERF deformation model classes can be viewed as converging from conceptual end members. The geologic models are source-based, in that they depend on the identification of all California faults and an assignment of slip rates on each of them. It is likely impossible that every fault can be identified, particularly since many are blind (buried faults with no surface traces), and some areas have been studied more intently than others. Completeness of the fault model is regionally dependent; compare, for example, the mapped fault density between northern and southern California in figure C2. Hazard-assessment results from these models might then be viewed as a minimum solution, unless correcting factors are made (that is, geodetically observed deformation zones; “C-zones”), which are also subject to uncertainty. Geodetically based deformation models represent the other end member; GPS observations record all crustal movements whether they are interseismic loading, aseismic creep, or postseismic deformation.

Much of the signal not believed to be seismogenic loading can be corrected for, but it is subject to uncertainty.

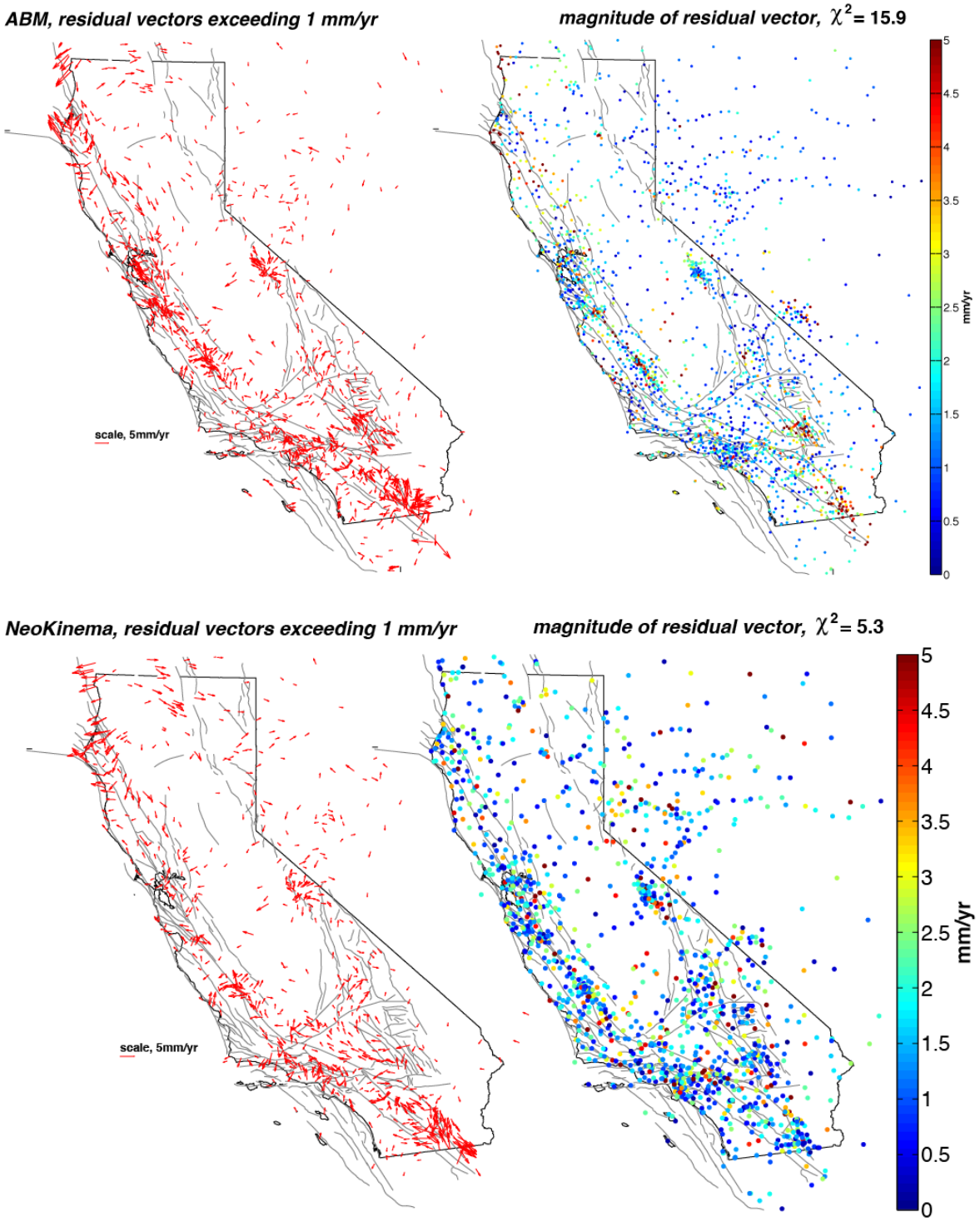

Figure C12. Vector maps of residuals to GPS observations for the three geodetic models.

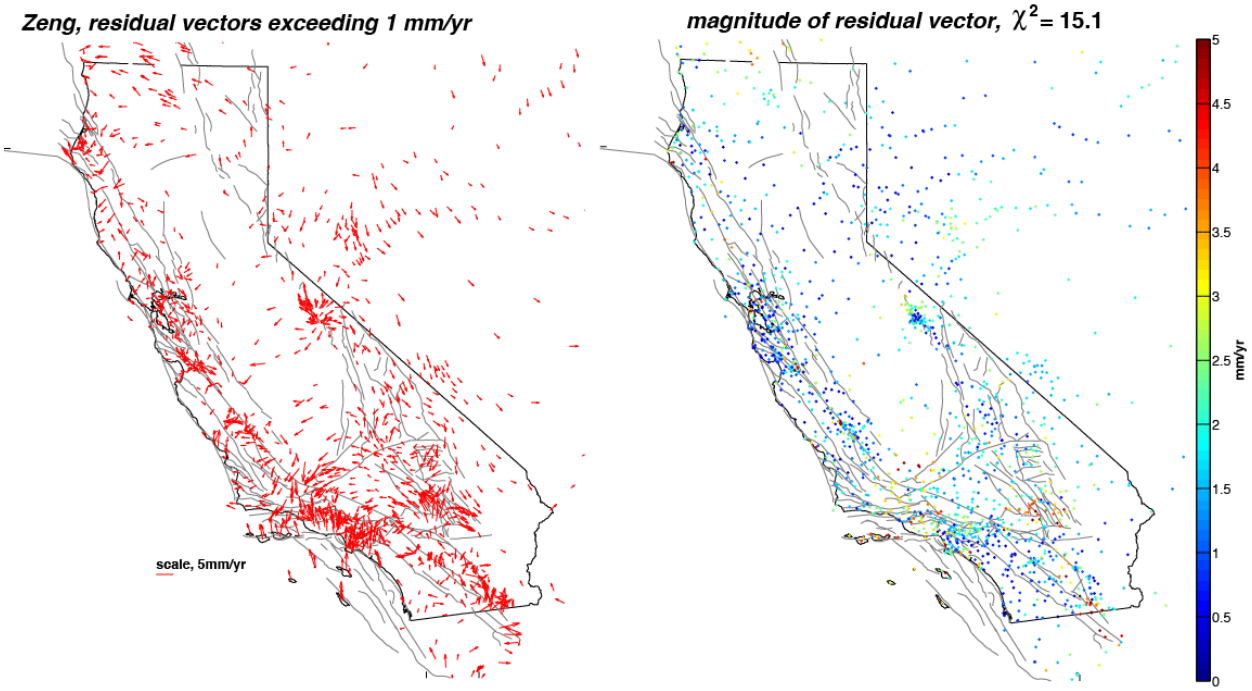

Figure C12-continued. Vector maps of residuals to GPS observations for the three geodetic models.

For comparison, the moment rate can be inferred directly from the GPS data, independent of assumptions used to create UCERF3 deformation models. The strain-rate tensor for all of California is computed using the GPS data and then converted to scalar moment rate using the same formula that was used for the off-fault moment rate in the deformation models (Savage and Simpson, 1997). In other words, all model assumptions about how GPS data are mapped into fault slip rate and other computations are stripped out, and GPS data are used to directly compute moment rate in the crustal volume. The result is shown in figure C13. The summed moment rate for the entire region is 3.03×10^{19} Nm/yr. This estimate is slightly on the high end because creep on the central San Andreas Fault and the Hayward Fault is not being accounted for correctly, and it is evident that high moment rates are bleeding off into the region outside of data constraints. However, this simple moment-rate calculation agrees quite well with the deformation model results (table C3). This confirms that the GPS data themselves are primarily the cause of relatively higher values of modeled moment rate and not the modeling methods used to make the UCERF3 deformation models.

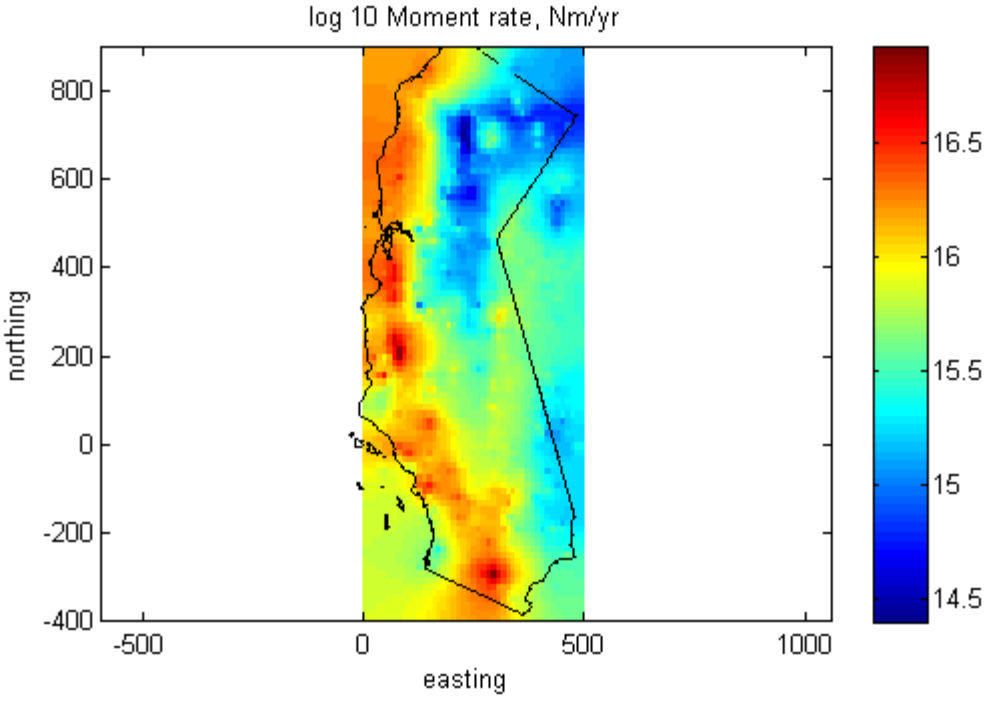

Figure C13. Map of the spatial distribution of total moment rate based on direct conversion from surface strain measured by GPS data using the method of Savage and Simpson (1997). Cumulative moment release from this exercise is consistent with UCERF3 deformation model results. Axes are scaled in km.

The end-member nature of the deformation modeling strategies is not necessarily reflected when the total seismic moment is calculated on faults for different models. Table C3 shows the cumulative annual moment rates for the five models being discussed. The UCERF2 solution, which is recognized as having an incomplete fault and slip-rate description, has the lowest moment rate on faults. The next higher are the Zeng-Shen and NeoKinema models, which have essentially the same on-fault moment rates. The UCERF3 geological and average block models are also about equal, but ~10 percent higher than the other two models (table C3). Thus, although an important implication of using the new UCERF3 deformation models is that they imply an overall moment-rate increase of as much as 24 percent, this is driven entirely by inclusion of new faults, rather than by use of geodetic models. Table C4 lists the most important new faults (slip rate >1 mm/yr).

From examination of table C3, there is a distinction that can be made between the elastic block model solution and the faulted continuum models. The overall moment release implied by the average block model is higher at 24 percent increase over UCERF2 compared with 8–12 percent increases implied by the faulted continuum solutions. This is caused by a greater percentage of moment rate on faults and an accompanying higher off-fault moment rate.

Table C3. Moment rates $\dot{M}_0$ ($\dot{M}_0$, given in units of 10^{19} Nm/yr) for the UCERF3 deformation models, plus implied values of maximum magnitude (M_{max}) and mean recurrence interval (MRI) of $M \geq 8$ events[6].

[Value includes fault-specific downdip widths and creep-based moment-rate reductions; default is 0.1 where no creep data exist. For reference, the average lower seismogenic depth is ~12 km in the UCERF3 Fault Models; with surface creep the average seismogenic thickness is ~11 km. The values in parenthesis are the moment-rate contributions from the more than 150 new fault sections added in UCERF3 (not included in UCERF2). For the Geologic model with Fault Model 3.1, 57 percent of the increase in parentheses is from the following three new faults: Cerro Prieto (0.077 × 1019 Nm/yr); Mendocino (0.054 × 1019 Nm/yr); and Brawley (Seismic Zone) alt 1 (0.049 × 1019 Nm/yr). Note that UCERF3 does not include most of the UCERF2 "Non-CA Faults"; contributions from these are "off fault" here. The value of 1.73 listed for UCERF2 has a 10-percent reduction for small earthquakes and aftershocks, but this is compensated by UCERF3 applying a default aseismicity of 0.1]

Fault Model	Deformation Model	Fault $\dot{M}_0$[1] (new faults)	$\dot{M}_0$ Off Faults[2]	% Off Faults	Total $\dot{M}_0$ (seismic and off-fault aseismic)	Total $\dot{M}_0$ Increase over UCERF2[3]	$\dot{M}_0$ Change on UCERF2 faults[4]	M_{max}[5]	MRI $M \geq 8$[5]
3.1	Average Block Model	2.02/(0.39)	0.93	31%	2.95	24%	-6%	8.36	205
	Geologic	2.00/(0.31)[4]	0.95	32%	2.95	24%	-3%	8.36	205
	NeoKinema	1.86/(0.42)	0.80	30%	2.66	12%	-16%	8.27	249
	Zeng-Shen	1.86/(0.30)	0.71	28%	2.57	8%	-10%	8.24	272
3.2	Average Block Model	2.02/(0.42)	0.92	31%	2.94	24%	-7%	8.36	205
	Geologic	2.00/(0.33)[4]	0.94	32%	2.94	24%	-3%	8.36	205
	NeoKinema	1.84/(0.42)	0.80	30%	2.64	11%	-18%	8.26	254
	Zeng-Shen	1.85/(0.31)	0.71	28%	2.56	8%	-11%	8.23	275
2.1	UCERF2	1.73/(0.0)	0.64	24%	2.37	0%	0%	8.15	385

[1]Values from K. Johnson's analysis of off-fault strain rates, which assume a seismogenic thickness of 11 km. The exception is the Geologic model, for which there is no off-fault strain rate map; its value was computed assuming the total moment rate for the Ave Block Model is correct (0.95 = 2.95-2.00 for UCERF3 FM 3.1). The UCERF2 value includes contributions from both "C-Zones (aseismic)" and "Non-CA Faults", the latter because most of the "Non-CA Faults" have been excluded in UCERF3.

[2]Relative to the UCERF2 total value of 2.37× 1019 Nm/yr, which includes contributions from "C-Zones (aseismic)". The UCERF3 on-fault values have aseismic contributions removed, but there may be aseismic contributions in the UCERF3 off-fault values.

[3]Comparison of on-fault moment rate for the same faults as used in the UCERF2 model.

[4]Implied values computed assuming a truncated GR distribution constrained to have the observed rate of 8.7 M ≥ 5 events per year and a b-value of 1.0.

[5]Values in this table compiled by running the following OpenSHA method on 10/12/12: UCERF3.analysis.DeformationModelsCalc.calcMoRateAndMmaxDataForDefModels().

Table C4. Listing of the highest slip-rate (>1 mm/yr) faults added to the UCERF3 model and their slip rates (in mm/yr) under the four different model formulations. All added faults and further details are listed in table C10.

Fault Section	Geo Rate	ABM rate	NeoKinema rate	Zeng-Shen rate
Cerro Prieto	35.00	34.62	9.42	14.37
Mendocino	35.00	48.13	48.81	35.60
Brawley (Seismic Zone) alt 1	23.00	22.50	27.08	23.67
Calaveras (So) Paicines extension	10.00	14.87	9.00	8.60
Hayward (So) extension 2011 CFM	8.00	8.22	5.90	10.17
Santa Susana alt 2	6.00	5.99	3.61	5.12
Santa Susana East (connector)	6.00	5.87	0.57	4.13
Mad River - Trinidad (alt2)	4.50	1.44	0.89	4.80
Hunting Creek - Bartlett Springs	3.00	7.16	4.71	8.30
Oak Ridge (Offshore) west extension	3.00	3.03	0.87	2.42
Owens Valley (Keough Hot Springs)	3.00	3.01	0.40	2.66
Sargent 2011 CFM	3.00	3.10	0.26	2.78
Garberville - Briceland 2011 CFM	2.60	11.96	2.62	2.25
San Jacinto (Lytle Creek connector)	2.50	2.50	0.37	2.31
Almanor 2011 CFM	2.20	2.14	0.85	2.07
Carson Range (Genoa)	2.00	2.14	1.64	1.54
Earthquake Valley (N extension)	2.00	1.94	0.11	1.72
Earthquake Valley (S extension)	2.00	1.99	0.33	1.75
Mt Diablo Thrust North	2.00	2.10	1.61	1.69
Mt Diablo Thrust South	2.00	2.25	1.36	1.63
San Andreas (North Branch Mill Creek)	2.00	2.00	1.92	1.71
San Diego Trough north alt1	2.00	1.93	1.38	3.19
San Diego Trough north alt2	2.00	1.93	1.89	2.43
San Diego Trough south	2.00	1.88	2.80	2.85
Great Valley 05 Pittsburg-Kirby Hills	1.80	1.78	0.25	1.48
Mission (connected) 2011 CFM	1.80	1.93	0.99	1.32
San Clemente	1.80	2.84	0.36	3.74
San Gorgonio Pass	1.80	1.75	0.71	2.23
Northridge Hills	1.30	0.25	0.90	1.49
Mission Hills 2011	1.25	1.14	0.65	1.05
Mission Creek	1.09	1.00	0.71	0.83
Antelope Valley 2011	1.00	1.03	1.89	0.97
North Channel	1.00	1.58	0.23	1.27
Oceanside alt1	1.00	0.77	0.42	0.88
Oceanside alt2	1.00	3.49	0.05	0.72
San Pedro Basin	1.00	1.05	1.49	1.47
Santa Cruz Catalina Ridge alt1	1.00	0.64	0.80	1.44
Santa Cruz Catalina Ridge alt2	1.00	0.64	0.70	1.34

The spatial distributions of off-fault moment release rates implied by the three geodetically based deformation models have features in common, but are also distinct from one another (figs. C14,15). All three models have more off-fault moment rate in southern California. The Zeng-Shen model has the smoothest distribution, whereas NeoKinema has the roughest (a function of the finite element grid used). The implications of applying UCERF3 geodetically derived background deformation rates with respect to UCERF2 would likely be higher hazards in the Great Valley, the Transverse Ranges, and southeast California (fig. C14).

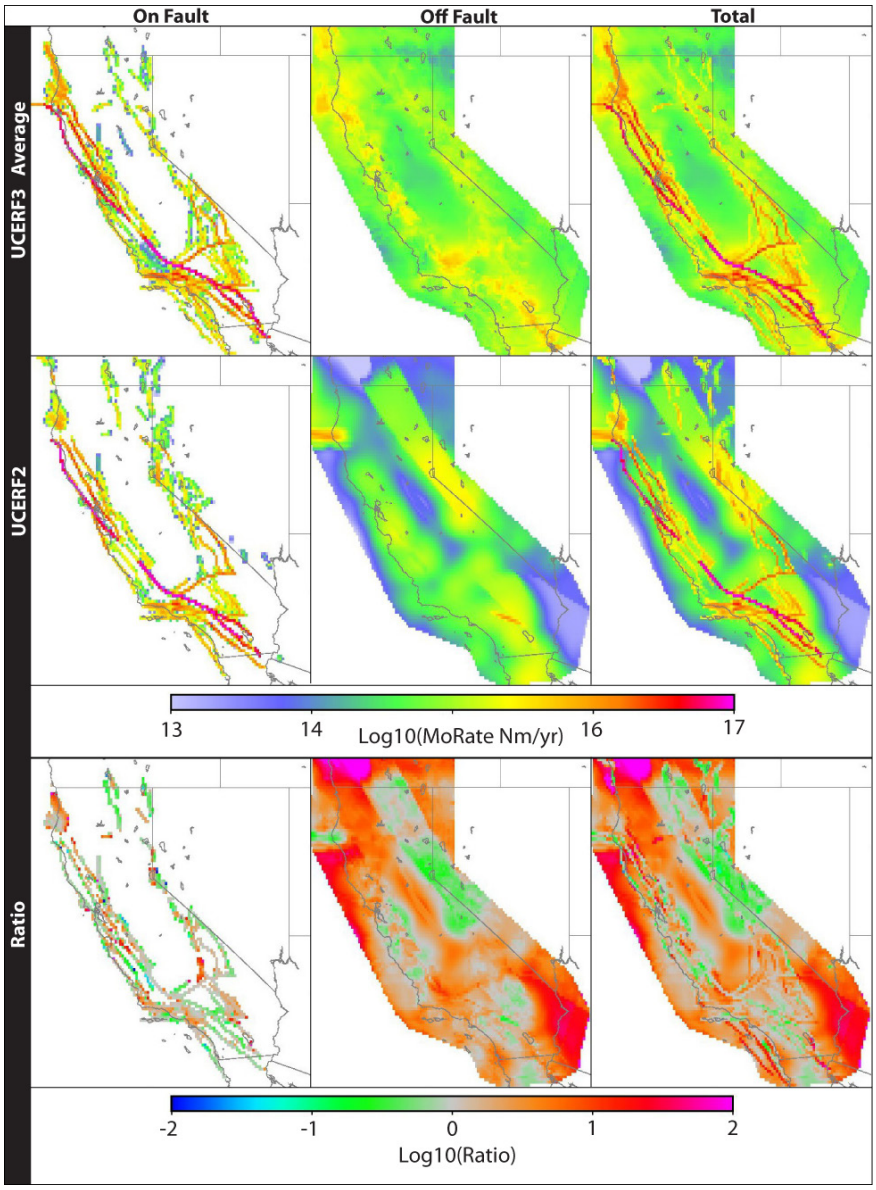

Figure C14. Maps comparing the average total UCERF3 moment rate, as well as the rates on and off defined fault zones, to the UCERF2 values.

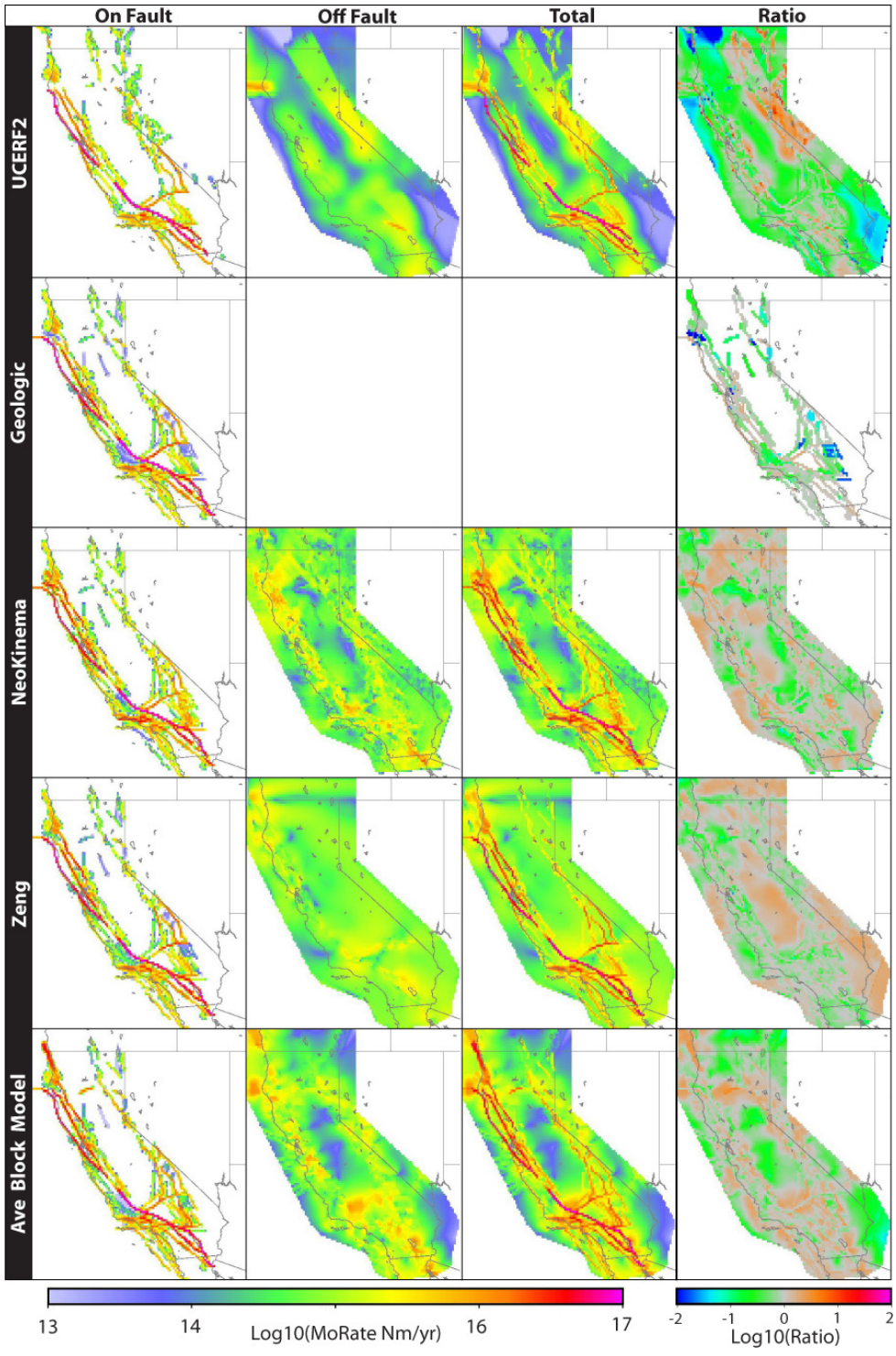

Figure C15. Maps comparing the individual UCERF3 deformation model moment rates and ratios to the average UCERF3 rates. The Geologic Model does not produce off fault deformation estimates, hence those fields are blank.

Because mapping moment rate may not be very intuitive in terms of comparing with slip rates, we calculated the implied fault slip from the residual off-fault moment rate grids for the three geodetic models. We show this component as cumulative slip rate against latitude in figure C16. The amount of slip assumed to occur on unknown faults is significant, reaching as much as 30 mm/yr at some latitudes in some models. This off-fault deformation is of course covariant with the calculated on-fault slip rates. It is also subject to considerable maximum magnitude uncertainty, as well as uncertainty in terms of the proportion that is aseismic.

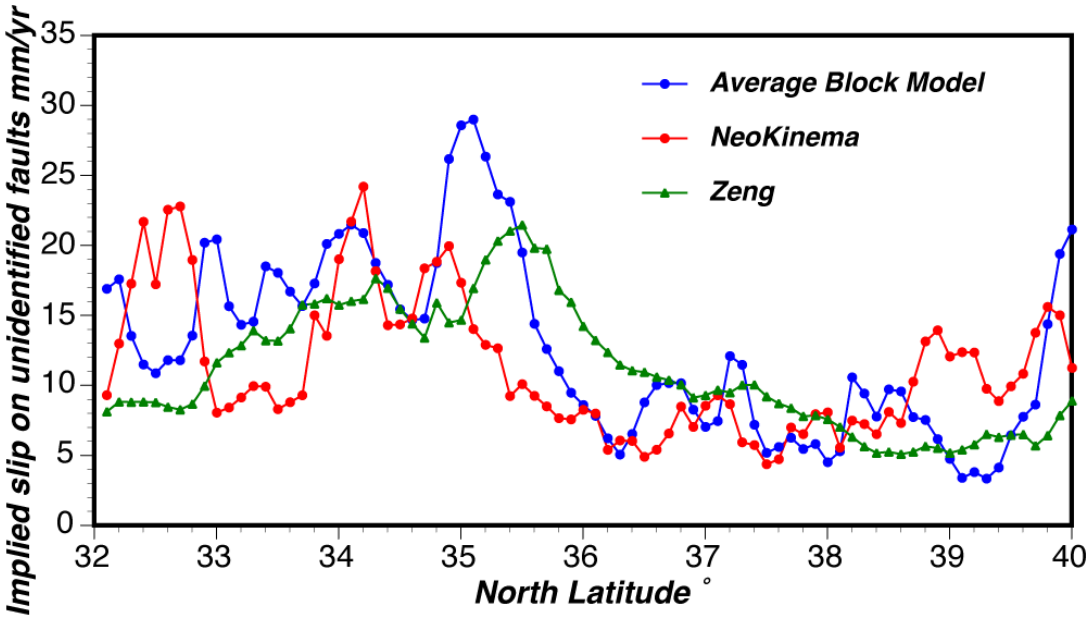

Figure C16. Plot of residual, off-fault moment rates converted to idealized slip rate on N34˚W trending vertical faults as a function of latitude. The purpose of this figure is to give a rough idea how much slip might be implied by the off-fault component in the geodetic deformation models.

As of this writing it remains undecided how the background moment release rates from geodetic solutions should be used or weighted. One option would be to only use their relative spatial distribution, but not the overall moment values because of uncertainty about aseismic deformation. The cumulative moment rate value in that scenario would be drawn from smoothed seismicity. Alternatively, some weight could be given to the geodetic solutions for off-fault deformation, which take into account the mechanical implications of the California fault system geometry in perhaps a more complete way than smoothed seismicity can. The overall moment rate is tied to assignment of regional maximum magnitude values, a topic outside the scope of this document. However, the tradeoffs between the assignment of moment release to major fault lines or to off-fault deformation can be potentially considered when weighing models. The average UCERF3 deformation model is compared with UCERF2 and UCERF3 smoothed seismicity in figure C17.

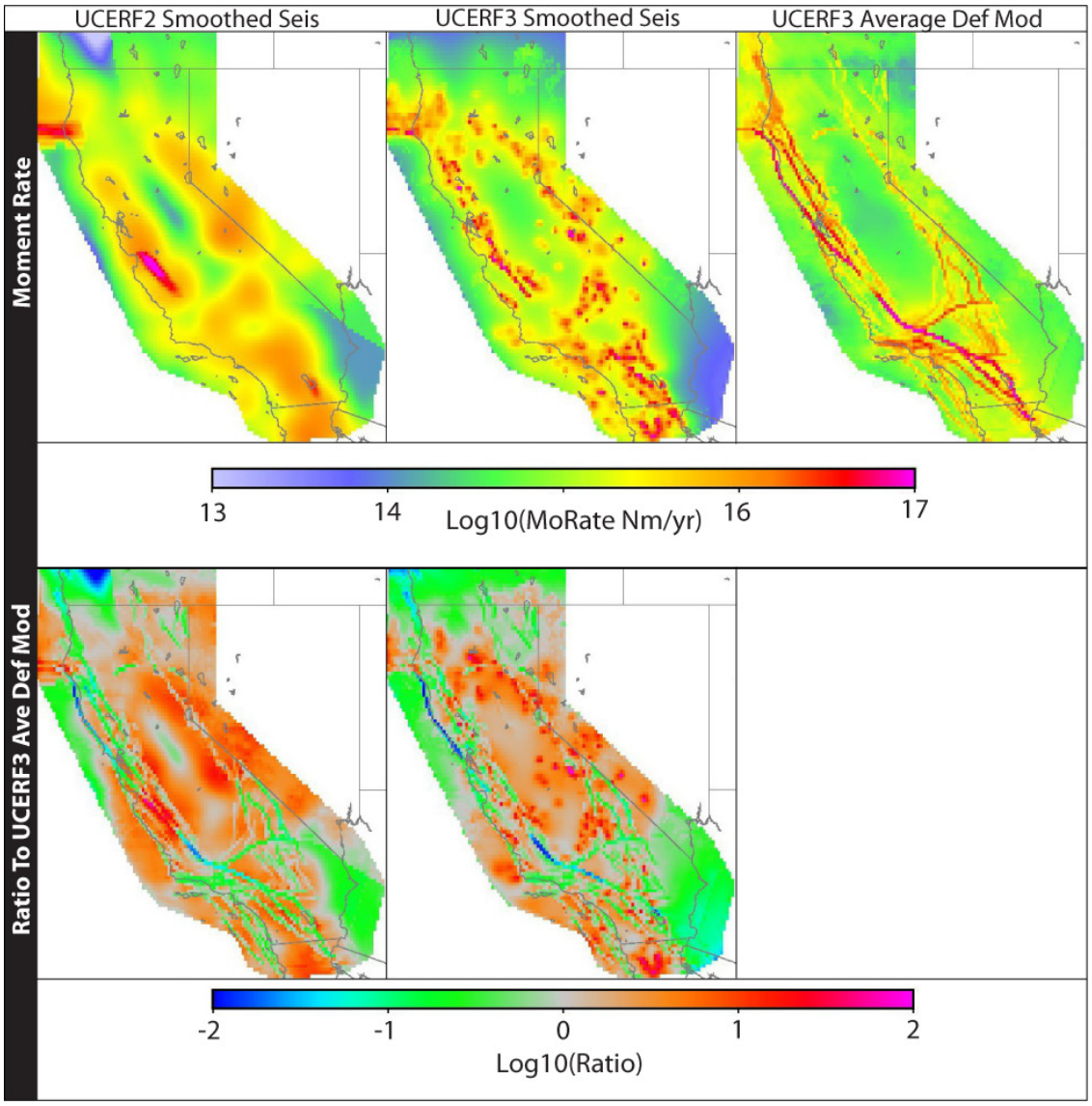

Figure C17. Maps comparing UCERF2 and UCERF3 smoothed seismicity approaches. Maps showing ratios to the average UCERF3 model highlight spatial differences between the geodetically derived off-fault deformation and that from seismicity.

The short period we have had to observe moment release in California causes significant uncertainty. We do not know how representative the ~150 year-instrumental and historical catalog is compared to the long term. The fact that deformation modeling is the preferred method to calculate earthquake rates over the empirical catalog is telling. Earthquake simulators may offer a glimpse in to the expected moment rate variability in California (Tullis and others, 2012). All models show moment rate variability by as much as a factor of three for 200-yr periods (fig. C18). Therefore reliance on fitting the instrumental moment-rate record could skew the long-term signal in the geologic and geodetic data.

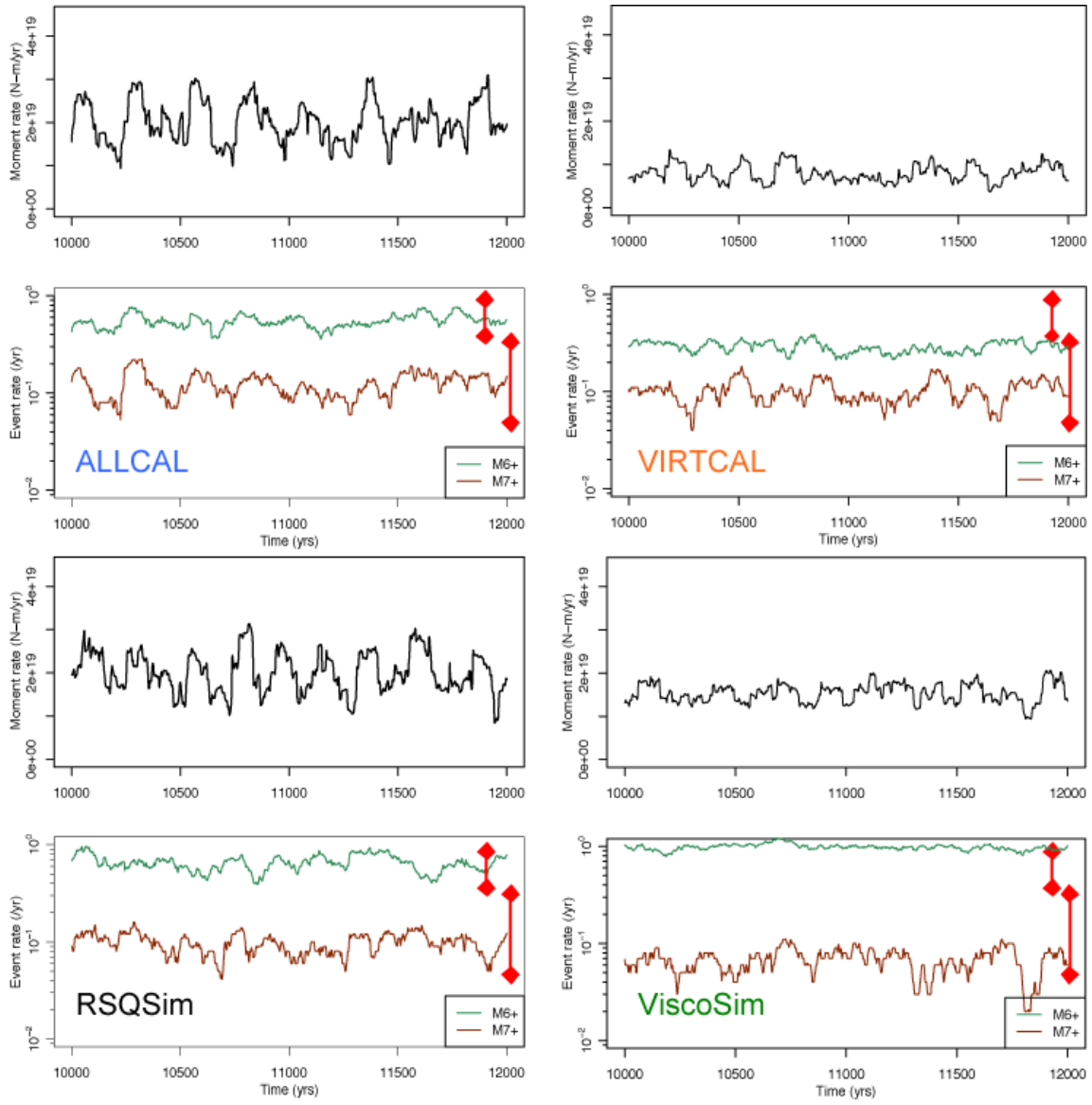

Figure C18. Graphs showing moment and event rates for a representative 2,000-year time span from 30,000-year simulations (Tullis and others, 2012); 100-year moving averages are plotted. Red bars show the observed 95-percent confidence intervals for *M*6+ and *M*7+ rates (Field and others, 2009). Note that simulated moment rates can differ by a factor of ~3 for periods of ~200 years, illustrating that the instrumental and historical records are too short to be representative samples of earthquake history.

Slip Rate Characterizations

Deformation models that are quantitatively constrained by geodetic observations are new to WGCEP and UCERF. We compared the UCERF3 geodetic solutions with the geologic model because geologically observed fault slip rates have been the primary input data to all past models. It should be noted that this is not equivalent to comparing with the UCERF2 deformation model, which combined geologic and geodetic data using expert opinion. These comparisons between UCERF3 models serve to highlight the differences between different models with different input and assumptions, rather than comparisons to a "correct" or even a "consensus" model.

Geologic observations of fault slip rates are clustered in California, with some faults having many nearby observations, and others few or none (fig. C2). The geologic models have fixed, extrapolated values along strike. The geodetic models are generally fixed within quoted uncertainties at locations where there are slip-rate observations, but are free to vary in between if the geodetic signal is a better fit. All modeling techniques attempt to conserve slip rate in the absence of changes necessary to fit GPS observations. However, slip-rate changes and gradients along strike are one of the phenomena typically not captured by point measurements from geology, and are thus one of the features we want to capture from geodesy.

There are differences in the smoothness in slip-rate solutions that depend on methods applied. In table C5, the highest slip rate (>5 mm/yr) faults are compared. The standard deviations in slip rate along same-named faults are calculated for FM3.1. The standard deviations in this instance are not implying errors, but are used to demonstrate model solution smoothness. The NeoKinema and Zeng-Shen models tend to have constant slip rates on the fastest faults, most with standard deviations of 0.0. The average block model solutions have more variability, with standard deviations ranging from zero to ~50 percent of geologic slip-rate values, though most are less than 10 percent (table C5). These variations occur between observed slip-rate values and are fit to GPS constraints. Thus there is no way to know whether a more constant slip rate or a variable-rate solution is correct. However, if a more constant slip rate solution is desired, then the faulted continuum solutions (NeoKinema, Zeng-Shen) appear to provide it, though the differences are small. Revisions to the average block model methods for calculating slip rates on off-block boundary faults has resulted in a much smoother solution than earlier versions.

Similar information is plotted in figure C19, where slip rate (mm/yr) is plotted against fault subsections for major California faults. In most, but not all, cases the geologic model has the highest slip rates of the four deformation models. A range of behaviors is displayed, from all four models lying within estimated geologic bounds, to along-strike slip-rate gradients, to all geodetic models falling below the geologic bounds. The Zeng-Shen model appears to be the geodetic solution that is nearest the geologic model, though not by much. In table C6, the mean misfit of the three geodetically constrained deformation models is given at the subsection level. The mean and 1σ values are well within the observation uncertainties for all three models.

Table C5. Comparison of along-strike slip rates for the highest slip rate faults in the UCERF3 fault model (FM3.1 used here). The standard deviation is calculated for the variation in slip rates amongst subsections on faults. Generally, the NeoKinema and Zeng-Shen models have smoother slip rates than the average block model.

	Standard deviation modeled slip rate (mm/yr)				
Fault Name	**ABM**	**NeoKinema**	**Zeng-Shen**	**Geological**	**Geological slip rate**
Mendocino	16.0	19.7	0.0	0.0	35.0
Imperial	3.3	0.0	0.0	0.0	35.0
Cerro Prieto	3.7	0.0	8.4	0.0	35.0
San Andreas (Cholame) rev	0.0	0.0	0.0	0.0	34.0
San Andreas (Big Bend)	1.9	0.0	0.0	0.0	34.0
San Andreas (Carrizo) rev	0.3	0.0	0.0	0.0	34.0
San Andreas (Creeping Section)	7.0	0.0	4.7	0.0	34.0
San Andreas (Mojave N)	6.8	0.0	0.0	0.0	32.5
San Andreas (Mojave S)	0.0	0.0	0.0	0.0	32.5
San Andreas (Offshore) 2011 CF	0.4	0.0	0.0	0.0	24.0
San Andreas (North Coast) 2011	0.1	0.0	0.0	0.0	24.0
San Andreas (San Bernardino N)	2.8	0.0	0.0	4.6	17.3
San Andreas (Peninsula) 2011 C	0.1	0.0	0.0	0.0	17.0
San Andreas (Santa Cruz Mts) 2	0.1	0.0	0.0	0.0	17.0
Calaveras (Central) 2011 CFM	4.3	0.0	0.0	0.0	15.0
Calaveras (So) 2011 CFM	0.1	0.0	0.0	0.0	15.0
San Jacinto (San Jacinto Valle	0.1	0.0	0.0	0.0	14.0
San Jacinto (Anza) rev	0.1	0.0	0.0	0.0	14.0
San Andreas (San Bernardino S)	0.7	0.0	0.0	0.0	13.0
San Jacinto (San Bernardino)	0.7	0.0	0.0	1.6	10.0
San Andreas (San Gorgonio Pass	5.5	0.0	0.0	0.0	10.0
Calaveras (So) - Paicines exte	2.3	0.0	0.0	0.0	10.0
Hayward (So) 2011 CFM	0.1	0.0	0.0	0.0	9.0
Hayward (No) 2011 CFM	0.2	0.0	0.0	0.0	9.0
Maacama 2011 CFM	0.9	0.0	0.0	0.0	9.0
Rodgers Creek - Healdsburg 201	0.3	0.0	0.0	0.0	9.0
Hayward (So) extension 2011 CF	0.3	0.0	0.0	0.0	8.0
Garlock (Central)	1.8	0.0	0.0	0.0	7.0
San Gregorio (North) 2011 CFM	0.3	0.0	0.0	0.0	7.0
San Jacinto (Coyote Creek)	0.1	0.0	0.0	0.5	6.7
Garlock (West)	0.6	0.0	0.0	0.8	6.6
San Jacinto (Clark) rev	1.4	0.0	0.0	1.8	6.3
San Jacinto (Superstition Mtn)	0.0	0.0	0.0	0.0	6.0
San Cayetano	0.1	0.0	0.0	0.0	6.0
Santa Susana alt 1	0.0	0.0	0.0	0.0	6.0
Calaveras (No) 2011 CFM	0.0	0.0	0.0	0.0	6.0
Santa Susana East (connector)	0.1	0.0	0.0	0.0	6.0
San Jacinto (Borrego)	0.2	0.0	0.0	0.0	5.0
Elsinore (Glen Ivy) rev	0.5	0.0	0.0	0.0	5.0

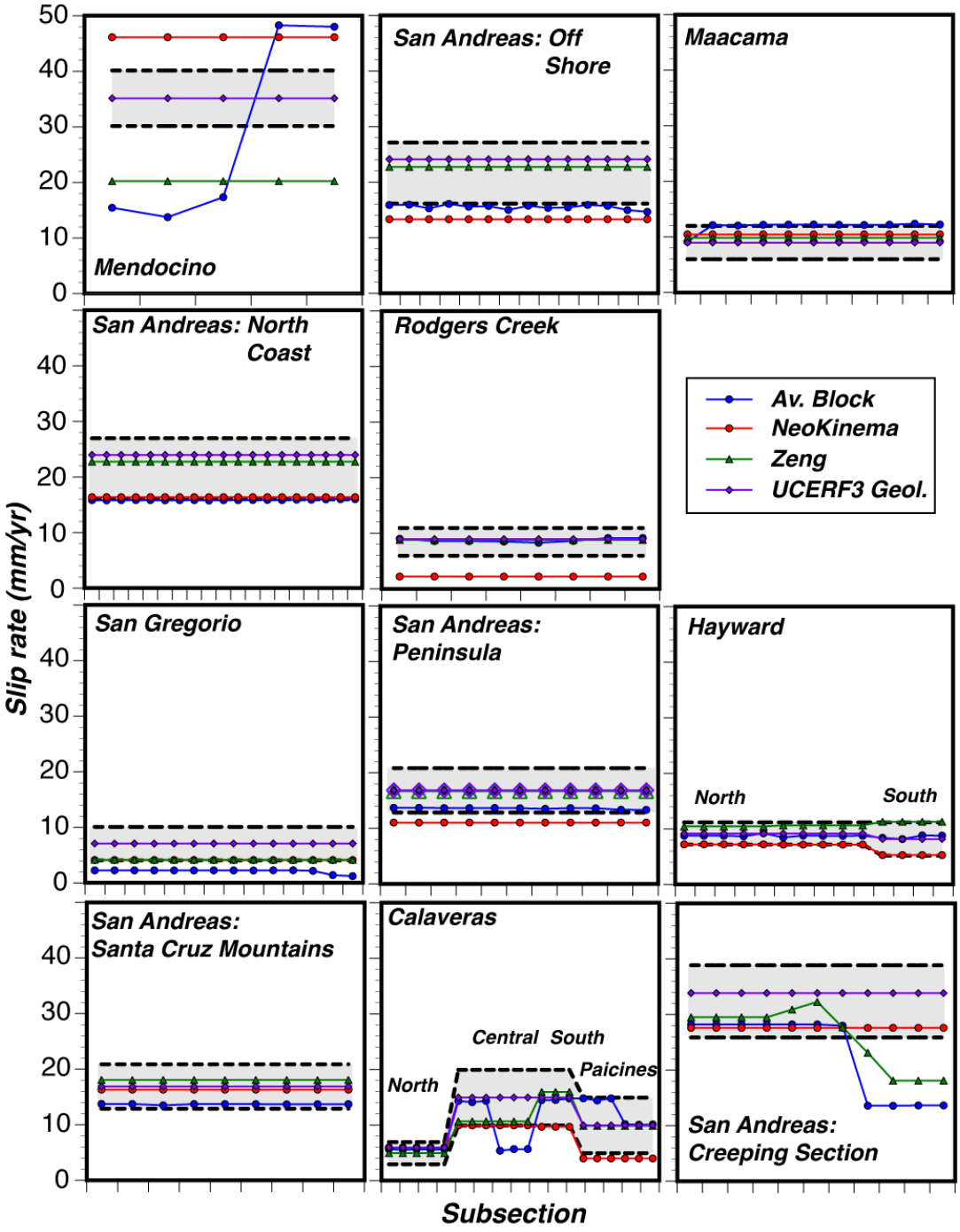

Figure C19. Plots of modeled slip rate (mm/yr) versus subsection on major California faults for four deformation models. Faults are plotted from north to south along strike beginning with northern California faults and moving to the south. The gray bands show the estimated geologic slip-rate bounds.

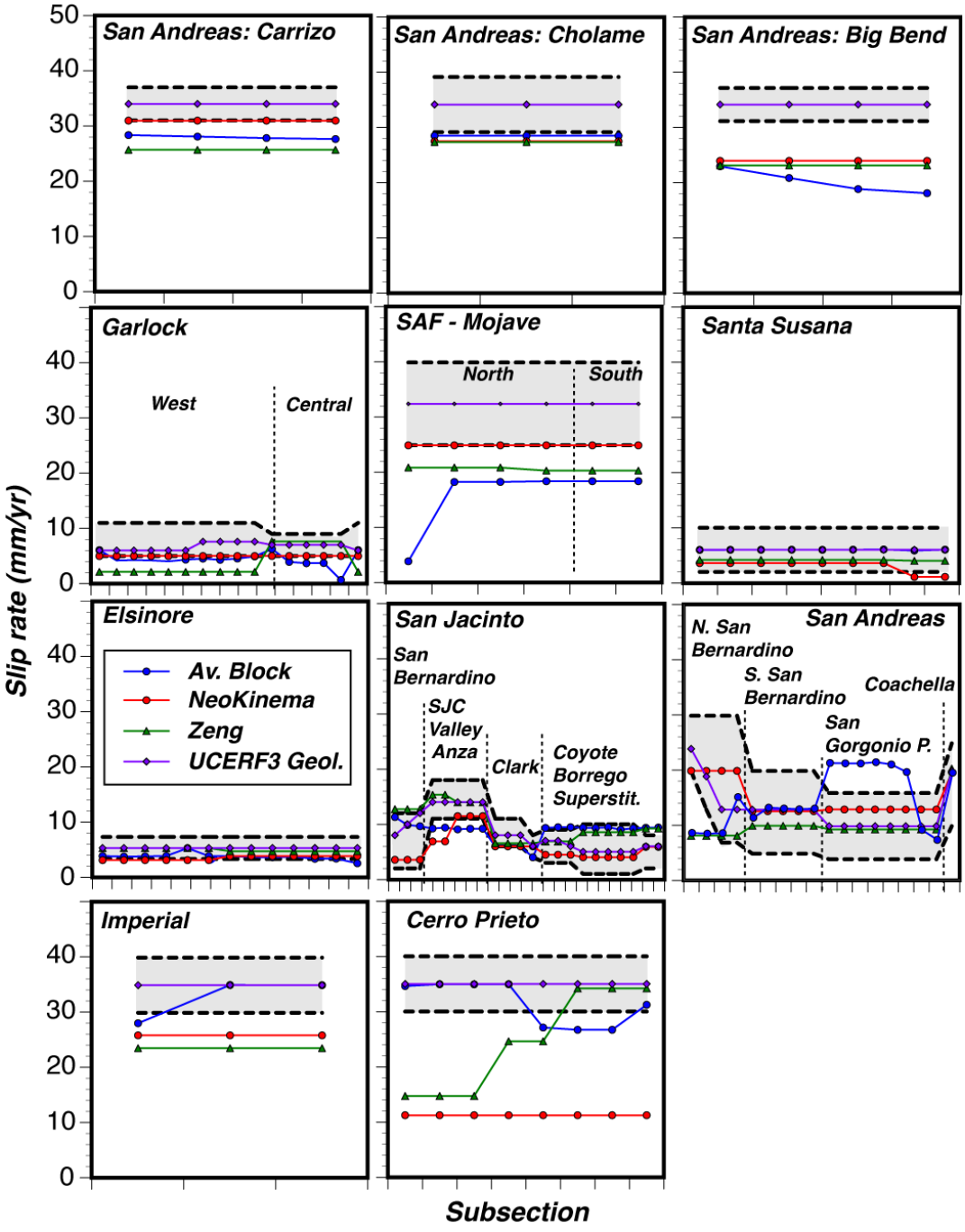

Figure C19. -continued. Plots of modeled slip rate (mm/yr) versus subsection on major California faults for four deformation models. Faults are plotted from north to south along strike beginning with northern California faults and moving to the south. The gray bands show the estimated geologic slip-rate bounds.

A potentially more robust geological observation might be the rake values in the grossest sense. For example, in most cases it should be fairly evident whether a dip-slip fault lies in an extensional or convergent terrane, or whether a strike-slip fault is right lateral or left lateral. We thus tallied the number of fault model subsections that had 180˚ differences from the geologically assigned rakes, which implies a complete reversal. As can be seen in table C6, the Zeng-Shen model is most closely associated with the geological rakes, followed closely by the average block model solutions. The average block model has the vast majority of subsections that are the same as the geological model, but it does have more reversals (12 subsections, depending on the fault model; table C6). Most of these reversals occur on relatively minor faults (fig. C20).

Table C6. Comparison of geodetically driven deformation model solutions with the UCERF3 geologic model. The Zeng-Shen model most closely matches the geologic model, both in terms of slip rates and rake directions. The average block model marks the largest departure from the geologic model. "FM3.1" and "FM3.2" refer to the two UCERF3 fault models.

FM3.1	***ABM***	***NeoKinema***	***Zeng-Shen***
Mean Δ slip rate from geological (mm/yr)	1.29	1.49	0.77
1σ	2.58	2.61	1.99
Maximum Δ from geological (mm/yr)	28.52	26.46	20.63
Mean rake Δ from geological (˚)	13.11	12.13	11.87
1σ	30.11	23.38	9.98
Number subsects. with 180˚ rake variation	12	3	0
FM3.2	***ABM***	***NeoKinema***	***Zeng-Shen***
Mean Δ slip rate from geological (mm/yr)	1.35	1.54	0.76
1σ	2.60	2.66	2.02
Maximum Δ from geological (mm/yr)	21.39	26.66	20.83
Mean rake variation from geological (˚)	14.22	13.11	11.65
1σ	31.04	25.39	9.99
Number subsects. With 180˚ rake variation	12	3	0

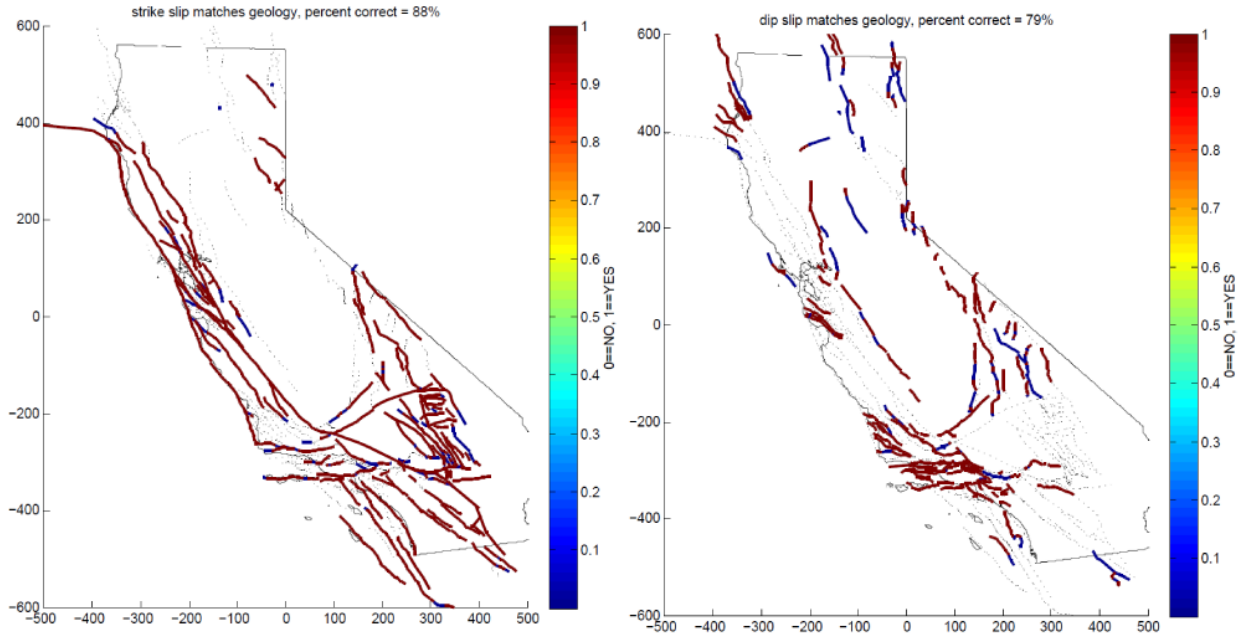

Figure C20. Maps showing geographic locations of average block model matches and mismatches to geologically observed or inferred rakes. Red faults are matched and blue are mismatched.

Covariance amid Parallel Strike-Slip Faults

Relatively closely spaced faults of similar rake that are locked can pose resolution problems in slip-rate modeling. The distribution of slip amongst the faults could vary significantly while producing similar geodetic signal. Long-term slip rates as determined from offset geologic features may not capture temporal changes in slip rates from interactions (see, for example, Marzocchi and Lombardi, 2008) and (or) mode switching (for example, Zöller and others, 2007; Hillers and others, 2009). The UCERF2 model had three realizations of deformation as a result of this issue, wherein the subparallel southern San Andreas and San Jacinto Faults were given covarying amounts of slip because published geologic and geodetic models (for example, Kendrick and others, 2002; Meade and Hager, 2005) have suggested approximately equal amounts of slip on the two faults, whereas past results showed more slip on the San Andreas Fault (Field and others, 2009).

We plot in figure C21 the slip rates from four UCERF3 deformation models on the covariant San Andreas and San Jacinto Faults. Slip-rate tradeoffs are more complex than those in the UCERF2 approach, with some models (like the average block model) placing more slip in the residual, off-fault areas at these latitudes. The range of UCERF3 deformation models therefore covers μ<5 mm/yr to μ>20 mm/yr of slip rate on each fault, compatible with the branches given in UCERF2 deformation models and other geologic and geodetic solutions (for example, Bennett and others, 2004; Fay and Humphreys, 2005; Meade and Hagar, 2005; Fialko, 2006).

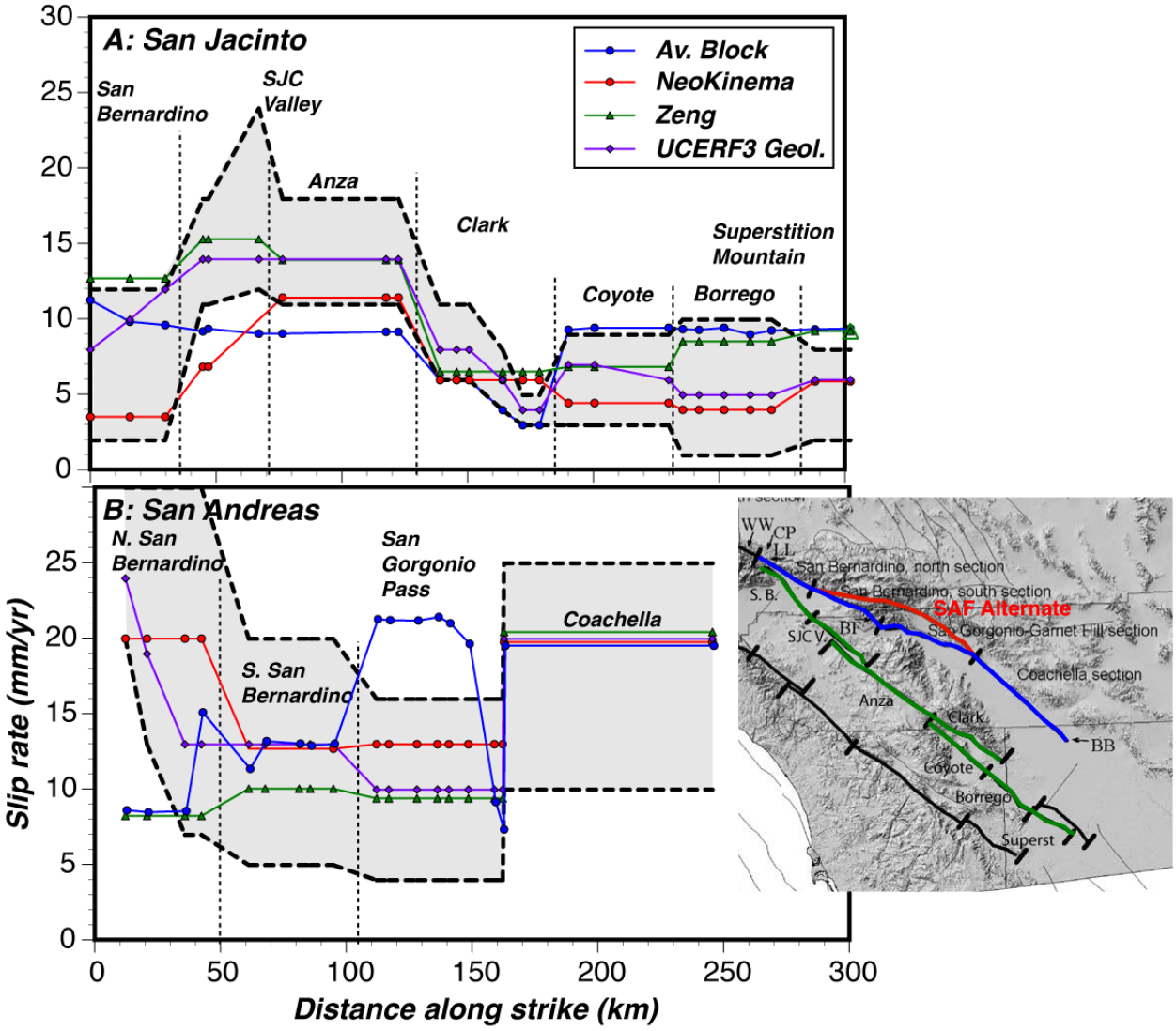

Figure C21. Plots of slip rate along strike on the subparallel southern San Andreas (a) and San Jacinto (b) Faults as determined by the different deformation models. These two faults represented the sole deformation model variation in UCERF2 because of a lack of consensus about whether the San Andreas is dominant, or whether the two faults have about equal slip. The range of models depicted here does allow for tradeoffs between these two faults, but the solutions are generally held within geologic bounds. This result suggests that the geologic and geodetic data are compatible in this area.

Line Integral Transects Through the Deformation Models

The geodetically constrained deformation models are expected to be cumulatively consistent with the relative motion between the Pacific and North American Plates, because they are constrained to fit the broad features of the GPS velocities that are calculated relative to stable North America (fig. C1). This is not the case for the UCERF3 geologic model. In similar fashion to the prior analyses, we examine the detailed, submodel-level solutions to examine local variability by summing slip rates on line integral paths directed orthogonally to the NUVEL-1

relative plate motion directions (DeMets and others, 1990, 2010) at 0.1˚ intervals in latitude through all the proposed UCERF3 deformation models as well as the UCERF2 model. We assume that the plate boundary deforms with a degree of uniformity over time. Thus a flawed model might show strong variability from section to section.

Deformation model transects are calculated by finding the east and north components of slip on each model fault, using the input geometry (strike, dip, dip-direction) and output slip rates and rakes. East and north components are summed along transects, and the implied motion vectors (magnitude and direction) are calculated. The off-fault deformation is not included in the transects to enable comparison with the UCERF3 geologic model and the UCERF2 deformation model. Creep and other aseismic slip on faults are included. We recognize that faults in the California region cannot fully represent the complete relative Pacific-North American Plate motion because, although much of this motion is accommodated in the San Andreas Fault system, a significant proportion is also taken up through Basin and Range Province oblique extension (see, for example, Parsons and Thatcher, 2011). Further complications result from the fact that a larger fraction of the southern part of California lies within the Basin and Range province, meaning more plate boundary motion is seen on integrals drawn at lower latitudes. Ultimately nearly all the relative plate motion is contained within the Salton Trough.

Results of model line-integral transects are shown in figures C22 and C23. The calculated values should be less than the whole relative plate motion (48±2 mm/yr) for the reasons stated above and because background moment accumulation is not included. However, because the San Andreas system is traversed by all the line integral paths, they ought to add up to most of the relative plate-motion vector associated with the given latitude (the actual value varies with position because plates rotate on a spherical Earth (see, for example, Argus and Gordon, 1990), and we assume that it would be smoothly varying. The wiggle plots of figures C22 and C23 show that none of our deformation models behave this way, a consequence of solutions that are dominated by discrete slip on discontinuous faults that bound elastic or less deformable regions or blocks.

Results of note from the summary of transects presented in figures C22 and C23 include that the UCERF2 solution falls in the middle of the range of UCERF3 models with the exception of southernmost California (south of 34˚N)—there new, high-slip-rate faults were added to the UCERF3 geologic model, whereas the UCERF2 model had an aseismic C-zone. Thus the geodetic solutions are not very different from UCERF2 in most of the state. The Zeng-Shen model is the most smoothly varying with latitude of all models (table C7). Other than in the Mendocino and Salton Sea regions, all the UCERF3 geodetic solutions actually produce less slip on faults than the UCERF2 and UCERF3 geologic models (fig. C24). A potential concern is that all models appear to have excessive amounts of slip rate where the Mendocino and north San Andreas Faults overlap, as well as where the Imperial and Cerro Prieto Faults overlap in the Salton Trough (figs. C24 and C25).

We have examined cumulative slip, but so far not direction. We thus made scatter plots of the angle from north of the net slip of each transect (made at 0.1˚ latitude intervals) across the deformation models. From table C7 it is apparent that all of our vectors trend a little more westerly (~4˚) than NUVEL-1. From the scatter plots shown in figure C24, it is apparent that nearly all mismatches from NUVEL-1 directions occur south of 33˚N for all deformation models. Perhaps not surprisingly, the more geological models (UCERF2, UCERF3 geologic, Zeng-Shen) tend to have the greatest proportion (46 percent) of misalignment from NUVEL-1.

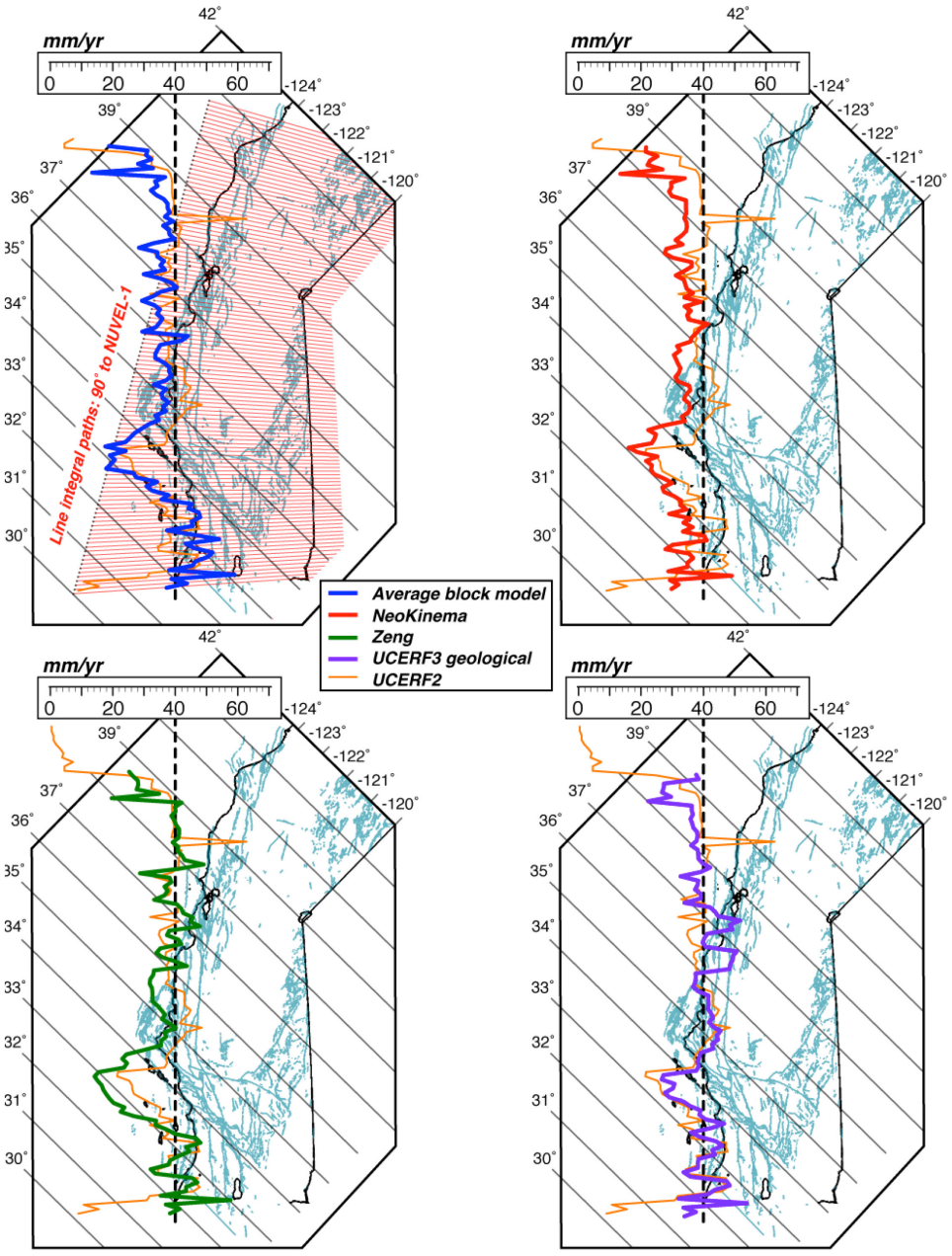

Figure C22. Separate plots of results from slip-rate transects using five different deformation models (the four under consideration for UCERF3 as well as UCERF2) overlaid on California map. Transects were computed at 0.1˚ intervals on lines oriented perpendicular to the NUVEL-1 relative plate motion directions (changes with latitude; Argus and Gordon, 2001). Red lines in upper left show integral paths. The heavy, dashed, black vertical lines show a 40-mm/yr reference slip rate. Hanging wall displacements were broken into north and east components and summed along the transects. Cumulative displacement rates (mm/yr) are plotted for each deformation model, and the UCERF2 rates are shown for comparison. The off-fault, background strain is not included in these calculations so that all the models can be directly compared.

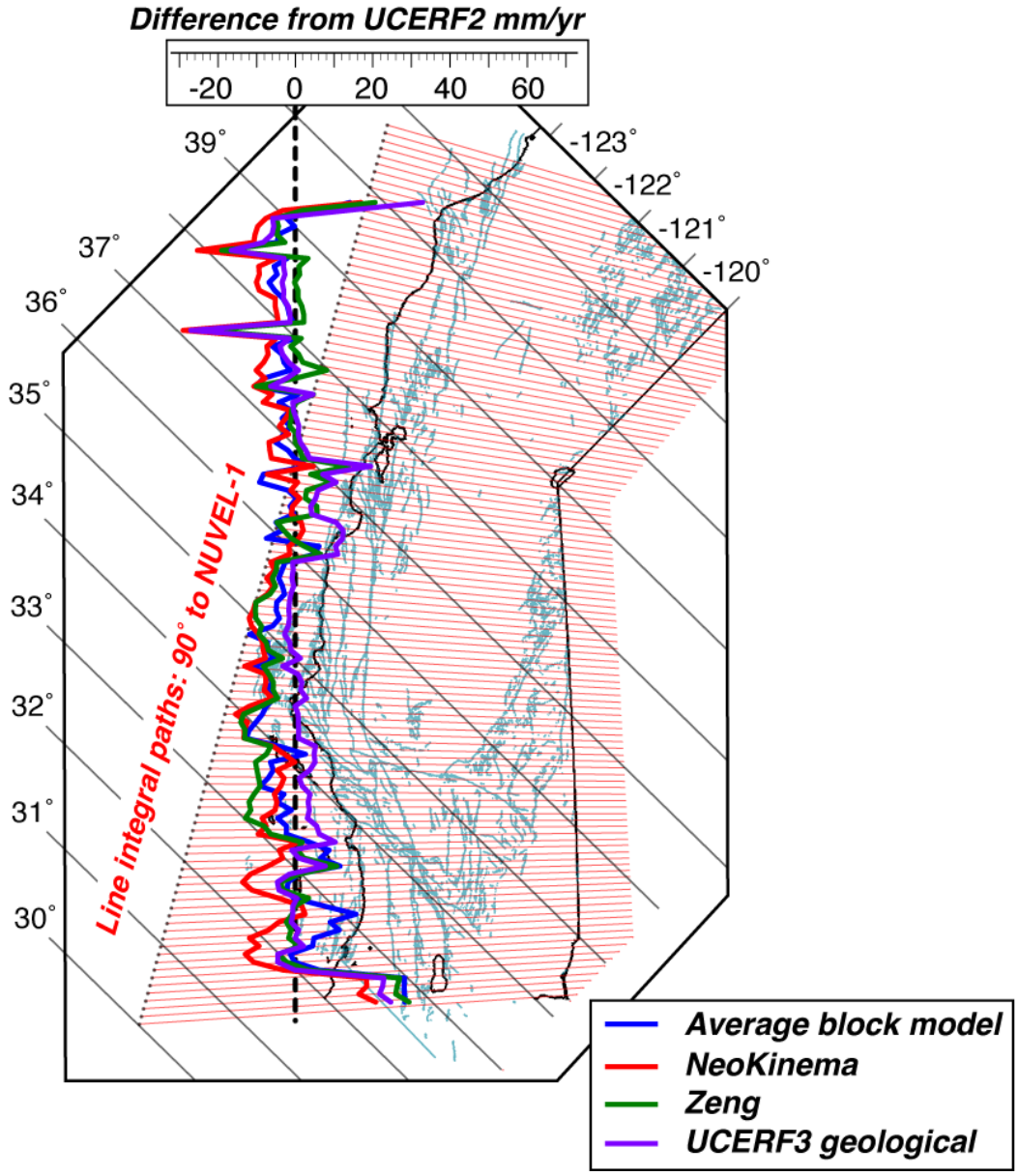

Figure C23. Plots of results of slip-rate transects as in figure C22, except here all UCERF3 model summed displacement rates are differenced from the UCERF2 rates. The heavy, dashed, black vertical line shows zero difference with UCERF2.

Table C7. Averages and standard deviations of directions and rates of displacement from transects across deformation models as shown in figures C22 and C23. The fractions of direction outliers from the NUVEL-1 model are given also.

	ABM	NeoKinema	Zeng-Shen	UCERF3 Geo.	UCERF2	NUVEL-1
Mean	N41.3˚W	N41.3˚W	N40.7˚W	N41.6˚W	N43.8˚W	N40.9˚W
1σ	10.0˚	11.8˚	11.2˚	12.2˚	13.0˚	
Fraction of transects out of NUVEL-1 range	41%	41%	43%	46%	46%	
Mean rate (mm/yr)	34.9	30.1	34.8	34.4	38.4	48
1σ (mm/yr)	7.7	7.0	8.9	12.7	6.0	

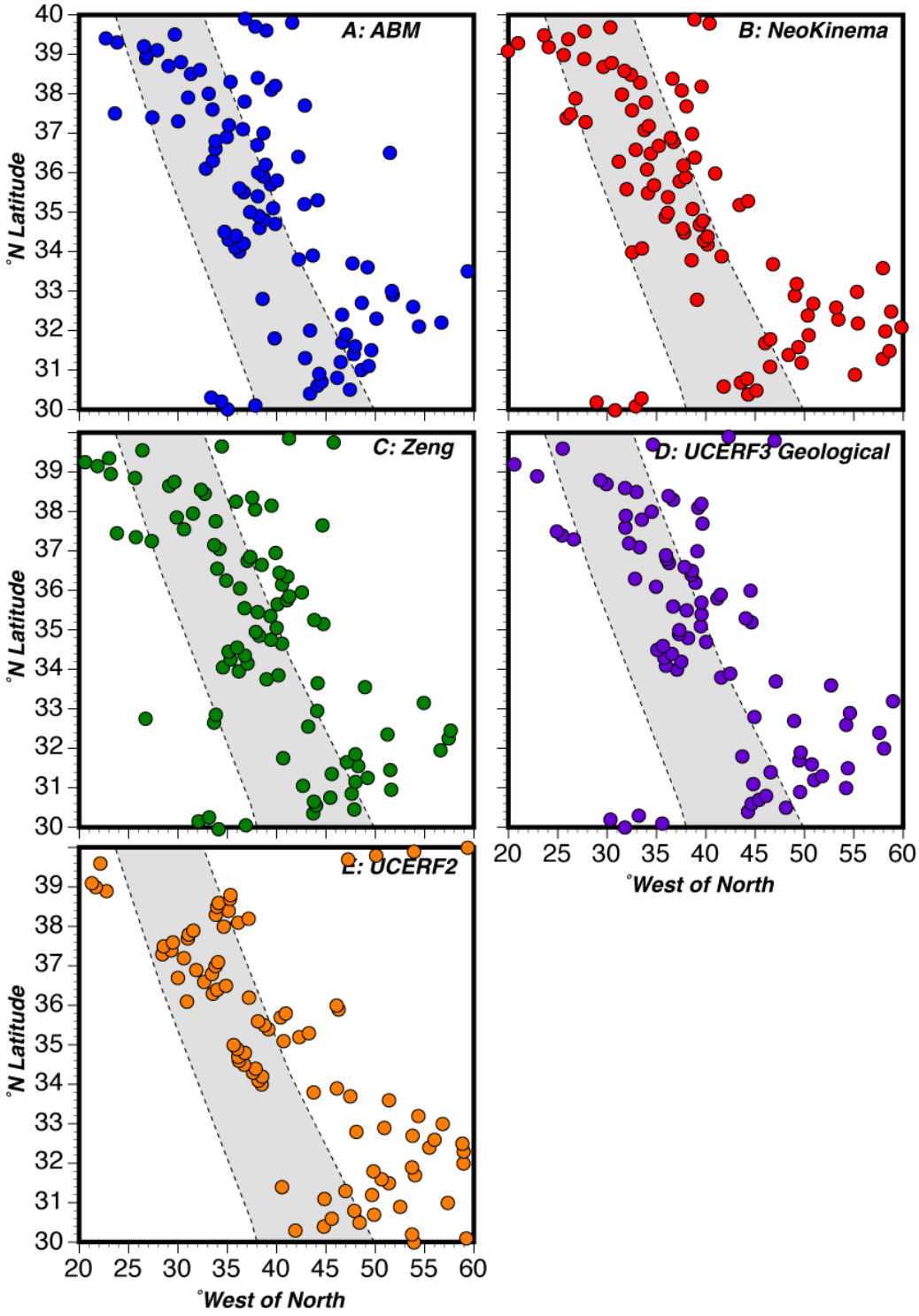

Figure C24. Map plots of slip direction (on defined faults only) from transects versus latitude. Shaded gray area shows North American-Pacific relative motion versus latitude from NUVEL-1 (Argus and Gordon, 1990).

Summary of Deformation Model Results

Here we summarize behaviors of different deformation models and rank them according to their performance against defined criteria that might be helpful in developing branch weights for the UCERF3 logic tree.

Total Moment Rate

All UCERF3 deformation models imply an increased moment release (8–24 percent increase) as compared with UCERF2. This results from a combination of additional fault sources that have been added and the use of geodetic data that record all current displacements, whereas primarily fault-based models are likely incomplete. If the moment discussion is limited to that on defined faults, then the UCERF3 geologic model represents a 17 percent increase over UCERF2, and the geodetic models represent a range of increase from 8 to 17 percent over the UCERF2 defined fault rate. If the discussion is limited to faults that were defined for both UCERF2 and UCERF3, then the new models all reduce the moment rate by 3–16 percent. Use of geodesy thus does not necessarily imply higher moment rates on defined faults (table C2). The UCERF2 model balanced the observed 150-yr seismic moment release rate. Thus adopting any of the UCERF3 deformation models without any aseismic deformation correction is an implicit statement that the 150-yr earthquake catalog is not completely representative of the longer term.

If one wishes to use the historical catalog fit as a ranking criterion, then the lowest moment-release rate models would be at the highest ranks as follows: (rank 1, tie) Zeng-Shen model and NeoKinema (both 1.86×10^{19} Nm/yr); (rank 2, tie) UCERF3 geological model (2.00×10^{19} Nm/yr), and average block model (2.02×10^{19} Nm/yr).

Fit to GPS Data

Ranking models by fit to GPS observations shows (rank 1) NeoKinema with reduced χ^2 value of 5.3; (rank 2) 15.1 for the Zeng-Shen model; (rank 3) average block model with reduced χ^2 value of 15.9; and (rank 4) no fit attempted for the UCERF3 geologic model. Ranking by spatial distribution of residuals can be performed on the basis of potential importance to loss calculations, in that the (rank 1) NeoKinema has the smallest residuals in Southern California and the San Francisco Bay region, (rank 2) the average block model is intermediate, and (rank 3) the Zeng-Shen model has the largest.

Slip on Faults

Examining the models in detail with regards to slip distributions and behavior on individual faults reveals the following characteristics. The average block model has more variable slip along faults, whereas the faulted continuum models have almost uniform slip on faults. In this sense the faulted continuum models behave most like the geology-only models of UCERF2 and the UCERF3 geologic model. The Zeng-Shen model in particular is most like the UCERF3 geologic model and is more weakly constrained by GPS.

A number of potential ranking factors apply. Ranking geodetic models by their overall fit to geology yields (rank 1) Zeng-Shen model with no rake reversals; (rank 2) NeoKinema with 3 rake reversals; and (rank 3) the average block model with 12. Similarly, ranking by overall fit to geologic slip rates yields (rank 1) Zeng-Shen model with smallest mean difference, followed by (rank 2) average block model and (rank 3) NeoKinema. Ranking models by

smoothness/continuity of slip rate on faster slipping (≥5 mm/yr) faults yields (rank 1) NeoKinema (smoothest); (rank 2) Zeng-Shen (intermediate); and (rank 3) average block model (roughest).

Line Integrals

Transects across the deformation models were drawn on paths orthogonal to the NUVEL-1 Pacific-North American relative plate-motion vectors at 0.1˚ latitude intervals. Hanging wall displacement vectors were found using calculated fault rates, rakes, and input fault geometry. Summing displacement shows variable net displacement direction and rate relative to the overall plate-motion vectors (NUVEL-1). The NeoKinema and average block model show the best fit to the plate-motion vectors because they are more influenced by geodesy.

Ranking can be described as (rank 1, tie) NeoKinema and the average block model each have 41 percent of relative plate-motion vectors from line integral paths outside of NUVEL-1 range; (rank 2) the Zeng-Shen model has 43 percent; and (rank 3) the UCERF geologic model has almost half outside at 46 percent.

Background Deformation

One measure of model performance is the amount of moment rate that it is necessary to put into background deformation off of defined faults. This can be viewed as the residuals of the modeling process. From table C3, we can rank the models on this measure as (rank 1) the NeoKinema model (0.79×10^{19} Nm/yr); (rank 2) the Zeng-Shen model (0.80×10^{19} Nm/yr); (rank 3) the average block model (0.93×10^{19} Nm/yr); and (rank 4) the UCERF3 geologic model, which does not attempt to balance this quantity.

Model Weighting

The UCERF process relies on a logic tree approach when confronted with multiple solutions or interpretations of the same data. The starting point has been to give equal weight to different models in the absence of information that defines a clear preference (Field and others, 2009). For UCERF3 we have three deformation models that use geology and geodesy and a fourth that is based solely on offset geological features. The purpose of this section is to determine if there was anything that emerged from the results that would cause us to not give equal weight to the four models.

As noted in previous sections, all the UCERF3 deformation models fit their intended input datasets at a reasonable degree of confidence. Therefore, additional criteria are identified here for consideration. These include (1) total moment release rate (directly impacts hazard); (2) fit to the GPS velocity field; (3) quantity of defined rake reversals on important faults, slip-rate solutions outside of well-constrained geologic bounds, and so forth; (4) consistency with relative plate-motion vectors; and (5) background moment rate off of defined faults.

The assortment of available models fall into two broad categories: (1) those tilting more to geologic constraints (UCERF3 geologic model, Zeng-Shen model) and (2) those tilting more toward geodetic constraints (average block model, NeoKinema). In the interest of capturing the aleatory uncertainty that is apparent on some of the most important, high-slip-rate faults like the San Andreas, one approach might be that combinations of the UCERF3 geology and Zeng-Shen models on the one hand and the average block model and NeoKinema on the other each add up to about 50 percent weighting.

If weighting is based on the model rankings given in the previous section of this report, then it can be broken into five categories: (1) total moment rate, (2) fit to GPS data, (3) characterization of slip rates on faults, (4) line integrals and consistency with the relative plate motions, and (5) moment rate distribution off defined faults. We can find the mean rank of each model from 1 to 4 in each category, with 1 being best, and assign points accordingly such that the best possible score would be 5, and the lowest, 20. If we do this, we find that the NeoKinema model has the best cumulative score of 8, followed by the Zeng-Shen model at 9, the average block model at 11, and the UCERF3 geologic model at 14. If these scores are normalized into weights, then it comes out that NeoKinema is weighted at 30 percent, Zeng-Shen 30 percent, the average block model at 20 percent, and the UCERF3 geologic model at 20 percent. This scheme gives roughly 50 percent weight to models that are more geodetic in nature (average block model, NeoKinema), and about 50 percent to geologic models (UCERF3 geologic, Zeng-Shen).

The UCERF3 Deformation Model Evaluation Committee's weights are summarized in table C8. For UCERF3.1 and UCERF3.2, the mean values of the committee's weighting were used, with average block model=0.2, NeoKinema=0.2, Zeng-Shen=0.3, and the UCERF3 geological model=0.3.

Table C8. Summary of relative model weighting as provided by the Deformation Model Review Committee members (listed here under "Reviewer" category).

	Model weights			
Reviewer	**ABM**	**NeoKinema**	**Zeng-Shen**	**UCERF3 Geology**
Dawson	0.25	0.25	0.30	0.20
Dieterich	0.10	0.20	0.10	0.60
Frankel	Lowest	Lowest	Medium	Highest
Parsons	0.20	0.30	0.30	0.20
Thatcher	0.40	0.20	0.20	0.25
Weldon	0.30	0.20	0.20	0.30
Wills	0.10	0.10	0.80	0.00
Mean	0.23	0.21	0.32	0.26
1σ	0.12	0.07	0.25	0.20
Interpretation for UCERF3.1				
Mean	0.2	0.2	0.3	0.3
Low	0.1	0.1	0.1	0.0
High	0.4	0.3	0.8	0.6

A result of the February 13–14, 2013, fault-by-fault review meetings was that the average block model (ABM), because it calculates deformation rates based on block-like behavior, has a tendency to exhibit higher slip rates along defined block boundaries than was deemed acceptable in many instances. The result of this is reduced ABM weight from 0.2 to 0.1. We do not support giving the ABM zero weight because there are data-driven reasons to conclude that block-like behavior occurs in the Earth (for example, Bennett and others, 1996; Prawirodirdjo and others, 1997; Souter, 1998; McClusky and others, 2001; Murray and Segall, 2001; McCaffrey, 2002, 2005; Meade and Hager, 2005; Simpson and others, 2012).

We therefore arrive at a final weight of ABM (0.10), NeoKinema (0.30), Zeng-Shen (0.30), Geology (0.30). We do this because the NeoKinema model represents a significantly better fit to GPS observations, with a normalized χ^2 misfit of 5.3, which is roughly a threefold

decrease compared with the ABM and Zeng-Shen models (15.9 and 15.1, respectively). All models were reviewed by expert panels for geologic consistency, and the NeoKinema model in particular was brought into consensus. The Zeng-Shen and geologic models combine to get 0.6 weighting, which tilts the solution toward geologic data constraints. However, we recognize that the geologic constraints on a significant fraction of California faults (~30 percent) are very weak to nonexistent, which was the primary reason to commission geodetic models.

Finally, the decision to doubly weight the paleo-rate constraint in the earthquake rate inversions adds additional geologic weighting on the type A faults. This has the effect of reducing geodetic influence on the major faults, particularly (and appropriately) where the geologic data are strongest. Therefore adding weight to NeoKinema has the primary effect of informing the earthquake rate model where geologic information is scarce.

References

Argus, D.F., and Gordon, R.G., 1990, Pacific-North American plate motion from very long baseline interferometry compared with motion inferred from magnetic anomalies, transform faults, and earthquake slip vectors: Journal of Geophysical Research, v. 95, p. 17315–17,324.

Argus, D.F., and Gordon, R.G., 2001, Present tectonic motion across the Coast Ranges and San Andreas fault system in central California: Geological Society of America Bulletin, v. 113, p. 1580–1592, doi:10.1130/0016-7606.

Bennett, R.A., Rodi, W., and Reilinger, R.E., 1996, Global Positioning System constraints on fault slip rates in southern California and northern Baja, Mexico: Journal of Geophysical Research, v. 101, p. 21943–21960.

Bennett, R.A., Friedrich, A.M., and Furlong, K.P., 2004. Codependent histories of the San Andreas and San Jacinto fault zones from inversion of fault displacement rates: Geology, v. 32, p. 961–964.

Bird, P., 2003, An updated digital model of plate boundaries: Geochemistry Geophysics Geosystems, v. 4, p. 1027, doi:10.1029/2001GC000252.

Bird, P., 2007, Uncertainties in long-term geologic offset rates of faults; general principles illustrated with data from California and other western states: Geosphere, v. 3, no. 6, p. 577–595; doi:10.1130/GES00127.1.

Bird, P., 2009, Long-term fault slip rates, distributed deformation rates, and forecast of seismicity in the western United States from joint fitting of community geologic, geodetic, and stress direction data sets: Journal of Geophysical Research, v. 114, no. B11, p. B11403, doi:10.1029/2009JB006317.

Bird, P., and Kagan, Y.Y., 2004, Plate-tectonic analysis of shallow seismicity; apparent boundary width, beta, corner magnitude, coupled lithosphere thickness, and coupling in 7 tectonic settings: Bulletin of the Seismological Society of America, v. 94, no. 6, p. 2380–2399, plus electronic supplement.

Bird, P., and Li , Y., 1996, Interpolation of principal stress directions by nonparametric statistics; global maps with confidence limits: Journal of Geophysical Research, v. 101, p. 5435–5443.

Bird, P., and Liu, Z., 2007, Seismic hazard inferred from tectonics: California: Seismological Research Letters, v. 78, no. 1, p. 37–48.

Brossy, C., Kelson, K., and Ticci, M., 2010, Digital compilation of data for the Contra Costa shear zone for the northern California quaternary fault map database; collaborative research with William Lettis & Associates, Inc. and the U.S. Geological Survey: Final Technical Report

submitted to the U.S. Geological Survey National Earthquake Hazard Reduction Program, Award Number 07HQGR0063; dated March, 2010, 20 p.

Bryant, W.A., 2000, Fault number 29, Bartlett Springs fault system, *in* Quaternary fault and fold database of the United States: U.S. Geological Survey Web site, accessed February 23, 2012, at *http://earthquakes.usgs.gov/regional/qfaults*.

Bryant, W.A., and Cluett, S.E., compilers, 1999, Fault number 54b, Calaveras fault zone, Central Calaveras fault section, in Quaternary fault and fold database of the United States: U.S. Geological Survey website, *http://earthquakes.usgs.gov/hazards/qfaults*.

Clark, D.G., and Slemmons, D.B., 1990, Late Pleistocene deformation in the Casmalia Hills region, coastal central California: Geological Society of America, Abstracts with Program, v. 22, no. 3, p. 14.

Clark, M.M., Harms, K.K., Lienkaemper, J.J., Harwood, D.S., Lajoie, K.R., Matti, J.C., Perkins, J.A., Rymer, M.J., Sarna-Wojcicki, A.M., Sharp, R.V., Sims, J.D., Tinsley, J.C., and Ziony, J.I., 1984, Preliminary slip-rate table for late Quaternary faults of California: U.S. Geological Survey Open-File Report 84–106, 12 p.

Coppersmith, K.J., 1979, Activity assessment of the Zayante-Vergeles fault, Central San Andreas fault system, California: Santa Cruz, University of California, Ph.D. dissertation, 216 p.

DeMets, C., Gordon, R.G., Argus, D.F., and Stein, S., 1990, Current plate motions: Geophysical Journal International, v. 101, no. 2, p. 425–478.

DeMets, C., Gordon, R.G., and Argus, D.F., 2010, Geologically current plate motions: Geophysical Journal International, v. 181, p. 1–80, doi:10.1111/j.1365-246X.2009.04491.x.

Fay, N.P., and Humphreys, E.D., 2005, Fault slip rates, effects of elastic heterogeneity on geodetic data, and the strength of the lower crust in the Salton Trough region, southern California: Journal of Geophysical Research, v. 110, no. B09401, doi:10.1029/2004JB003548.

Fialko, Y., 2006, Interseismic strain accumulation and the earthquake potential on the southern San Andreas fault system: Nature, v. 441, p. 968–971, doi:10.1038/nature04797.

Field, E.H., Dawson, T.E., Felzer, K.R., Frankel, A.D., Gupta, V., Jordan, T.H., Parsons, T., Petersen, M.D., Stein, R.S., Weldon, R.J., II, and Wills, C.J., 2009, The uniform California earthquake rupture forecast, version 2 (UCERF 2): Bulletin of the Seismological Society of America, v. 99, p. 2053–2107, doi:10.1785/0120080049.

Hammond, W.C., Blewitt, G., and Kreemer, C., 2011, Block modeling of crustal deformation of the northern Walker Lane and Basin and Range from GPS velocities: Journal of Geophysical Research, v. 166, no. B04402, doi:10.1029/2010JB007817.

Hillers, G., Carlson, J.M., and Archuleta, R.J., 2009, Seismicity in a model governed by competing frictional weakening and healing mechanisms: Geophysical Journal International, v. 178, p. 1363–1383.

Howe, T.C., and Bird, P., 2010, Exploratory models of long-term crustal flow and resulting seismicity in the Alpine-Aegean orogen: Tectonics, v. 29, no. TC4023, doi:10.1029/2009TC002565.

Hsu, Y.J., Ando, M., Yu, S.B., and Simons, M., 2012, The potential for a great earthquake along the southernmost Ryukyu subduction zone: Geophysical Research Letters, v. 39, L14302, doi:10.1029/ 2012GL052764.

Johnson, K.M., and Fukuda, J., 2010, New methods for estimating the spatial distribution of locked asperities and stress-driven interseismic creep on faults with application to the San

Francisco Bay area, California: Journal of Geophysical Research, v. 115, no. B12408, doi:10.1029/2010JB007703.

Kelson, K.I., Baldwin, J.N., Unruh, J.R., and Lettis, W.R., 2004, Coastal marine terraces define Late Quaternary fault activity and deformation within northern East Bay hills, San Francisco Bay region [abs.]: Eos (Transactions of the American Geophysical Union), v. 85, Fall Meeting Supplement, Abstract T13C-1396.

Kelson, K.I., Unruh, J.R., and Baldwin, J.N., 2005, Late Quaternary deformation in the northeastern East Bay hills, San Francisco Bay region [abs.]: Geological Society of America, Abstracts with Programs, v. 37, no. 4, p. 106.

Kendrick, K.J., Morton, D.M., Wells, S.G., and Simpson, R.W., 2002, Spatial and temporal deformation along the northern San Jacinto fault, southern California; implications for slip rates: Bulletin of the Seismological Society of America, v. 92, p. 2782–2802.

Kong, X., and Bird, P., 1995, SHELLS; a thin-plate program for modeling neotectonics of regional or global lithosphere with faults: Journal of Geophysical Research, v. 100, p. 22129–22131.

Liu, Z., and Bird, P., 2008, Kinematic modeling of neotectonics in the Persia-Tibet-Burma orogen: Geophsyical Journal International, v. 172, no. 2, p. 779–797, doi:10.1111/j.1365-246X.2007.03640.x

Marzocchi, W., and Lombardi, A.M., 2008, A double branching model for earthquake occurrence: Journal of Geophysical Research, v. 113, no. B08317, doi:10.1029/2007JB005472.

McCaffrey, R., 2002, Crustal block rotations and plate coupling, *in* Stein, S., and Freymueller, J., eds., Plate boundary zones: American Geophysical Union, Geodynamics Series, v. 30, p. 101–122.

McCaffrey, R., 2005, Block kinematics of the Pacific/North America plate boundary in the southwestern United States from inversion of GPS, seismological, and geologic data: Journal of Geophysical Research, v. 110, no. B07401, doi:10.1029/2004JB003307.

McClusky, S.C., Bjornstad, S.C., Hagar, B.H., King, R.W., Meade, B.J., Miller, M.M., Monastero, F.C., and Souter, B.J., 2001, Present-day kinematics of the eastern California shear zone from a geodetically constrained block model: Geophysical Research Letters, v. 28, p. 3369–3372.

Meade, B.J., and Hager, B.H., 2005, Block models of crustal motion in southern California constrained by GPS measurements: Journal of Geophysical Research, v. 110, no. B03403, doi:10.1029/2004JB003209.

Meisling, K.E., 1984, Neotectonics of the North Frontal fault system of the San Bernardino Mountains, southern California, Cajon Pass to Lucerne Valley—Pasadena: Pasadena, California Institute of Technology, Ph.D. dissertation, 394 p., 2 plates, scale 1:24,000.

Murray, M.H., and Segall , P., 2001, Modeling broad scale deformation in northern California and Nevada from plate motions and elastic strain accumulation: Geophysical Research Letters, v. 28, p. 4315–4318.

Okada, Y., 1985, Surface deformation due to shear and tensile faults in a half-space: Bulletin of the Seismological Society of America, v. 75, p. 1135–1154.

Okada, Y., 1992, Internal deformation due to shear and tensile faults in a half-space: Bulletin of the Seismological Society of America, v. 82, p. 1018–1040.

Parsons, T., and Thatcher, W., 2011, Diffuse Pacific-North American plate boundary—1000 km of dextral shear inferred from modeling GPS data: Geology, v. 39, p. 943–946, doi:10.1130/G32176.

Peltzer, G., and Tapponnier, P., 1988, Formation and evolution of strike-slip faults, rifts, and basins during the India-Asia collision; an experimental approach: Journal of Geophysical Research, v. 93, p. 15085–15117.

Perkins, J.A., and Sims, J.D., 1988, Late Quaternary slip along the Calaveras fault near Hollister, California: Eos (Transactions of the American Geophysical Union), v. 69, no. 44, p. 1420.

Prawirodirdjo, L., Bock, Y., McCaffrey, R., Genrich, J., Calais, E., Stevens, C., Puntodewo, S.S.O., Subarya, C., Rais, J., Zwick, P., and Fauzi, 1997, Geodetic observations of interseismic strain segmentation at the Sumatra subduction zone: Geophysical Research Letters, v. 24, p., 2601–2604.

Ryberg, T., Haberland, C., Fuis, G.S., Ellsworth, W.L., and Shelly, D.R., 2010, Locating non-volcanic tremor along the San Andreas fault using a multiple array source imaging technique: Geophysical Journal International, v. 183, p. 1485–1500, doi:10.1111/j.1365-246X.2010.04805.x

Savage, J.C., and Burford, R.O., 1973, Geodetic determination of relative plate motion in central California: Journal of Geophysical Research, v. 78, p. 832–845.

Savage, J.C., and Simpson, R.W., 1997, Surface strain accumulation and the seismic moment tensor: Bulletin of the Seismological Society of America, v. 87, p. 1345–1353.

Schmidt, K.M., Langenheim, V.E., Hanshaw, M.N., Miller, D.M., Hillhouse, J.W., and Phelps, G.A., 2010, Geology and geophysics illuminate late Quaternary offset along the Cady fault within the eastern California shear zone, southern California [abs.]: Geological Society of America Abstracts with Program, v. 42, no. 4, p. 83.

Schwartz, D.P., Pantosti, D., Hecker, S., Okumura, K., Budding, K.E., and Powers, T., 1992, Late Holocene behavior and seismogenic potential of the Rodgers Creek fault zone, Sonoma County, California, *in* Borchardt, G., Hirschfeld, S.E., Lienkaemper, J.J., McClellan, P., Williams, P.L., and Wong, I.G., eds., Proceedings of the Second Conference on Earthquake Hazards in the eastern San Francisco Bay area: California Division of Mines and Geology Special Publication 113, p. 393–398.

Shelly, D.R., and Hardebeck, J.L., 2010, Precise tremor source locations and amplitude variations along the lower-crustal central San Andreas fault: Geophysical Research Letters, v. 37, no. L14301, doi:10.1029/2010GL043672.

Shelly, D.R., and Johnson, K.M., 2011, Tremor reveals stress shadowing, deep postseismic creep, and depth-dependent slip recurrence on the lower-crustal San Andreas fault near Parkfield: Geophysical Research Letters, v. 38, no. L13312, doi:10.1029/2011GL047863.

Simpson, R.W., Thatcher, W., and Savage, J.C., 2012, Using cluster analysis to organize and explore regional GPS velocities: Geophysical Research Letters, v. 39, no. L18307, doi:10.1029/2012GL052755.

Souter, B.J., 1998, Comparisons of geological models to GPS observations in southern California: Cambridge, Massachusetts Institute of Technology, Ph.D. dissertation, p. 85.

Thatcher, W., 2009, How the continents deform—the evidence from tectonic geodesy: Annual Review of Earth and Planetary Sciences, v. 37, p. 237–262.

Tullis, T.E., Richards-Dinger, K., Barall, M., Dieterich, J.H., Field, E.H., Heien, E.M., Kellogg, L.H., Pollitz, F., Rundle, J.B., Sachs, M.K., Turcotte, D.L., Ward, S.N., and Yikilmaz, M.B., 2012, Comparison among observations and earthquake simulator results for the allcal2

California fault model: Seismological Research Letters, v. 83, p. 994–1006, doi:10.1785/0220120094.

Turcotte, D., and Schubert, G., 1982, Geodynamics: Hoboken, N. J., John Wiley, 450 p.

Unruh, J.R., and Kelson, K.I., 2002a, Critical evaluation of the northern termination of the Calaveras fault, eastern San Francisco Bay area, California: Final Technical Report submitted to the U.S. Geological Survey National Earthquake 13 Hazard Reduction Program, Award Number 00-HQ-GR-0082; dated July, 2002, 28 p.

Unruh, J.R., and Kelson, K.I., 2002b, Critical evaluation of the northern termination of the Calaveras fault, eastern San Francisco Bay area, California [abs.]: Eos (Transactions of the American Geophysical Union), Fall Meeting Supplement, abstract T62F-04, p. 1300.

Wentworth, C.M., Williams, R.A., Jachens, R.C., Graymer, R.W., and Stephenson, W.J., 2010, The Quaternary Silver Creek fault beneath the Santa Clara Valley, California: U.S. Geological Survey Open-File Report 2010–1010, 50 p., available at *http://pubs.usgs.gov/of/2010/1010/.*

Zeng, Y., and Shen, Z.K., Fault network modeling of crustal deformation in California constrained using GPS and geologic observations: submitted to Tectonophysics.

Zienkiewicz, O.C., 1977, The finite element method: New York, McGraw-Hill, 787 p.

Zöller, G., Ben-Zion, Y., Holschneider, M., and Hainzl, S., 2007, Estimating recurrence times and seismic hazard of large earthquakes on an individual fault: Geophysical Journal International, v. 170, p. 1300–1310.